Developmental Biology
Neuroscience

Semaphorin7A patterns neural circuitry in the lateral line of the zebrafish

Agnik Dasgupta, **Caleb C. Reagor**, **Sang P. Paik**, **Lauren M. Snow**, **Adrian Jacobo**, **A. J. Hudspeth**

Howard Hughes Medical Institute and Laboratory of Sensory Neuroscience, The Rockefeller University, New York, NY, USA • Tri-Institutional PhD Program in Computational Biology and Medicine, New York, NY, USA • Chan Zuckerberg Biohub San Francisco, San Francisco, CA, USA

A newer version is available. **Read the latest version**.

Version of Record
August 12, 2024

Reviewed Preprint
v3 • May 17, 2024

Reviewed Preprint
v2 • April 8, 2024

Reviewed Preprint
v1 • September 12, 2023
Not revised

eLife assessment

This study presents **valuable** findings on the roles of the axon growth regulator Sema7a in the formation of peripheral sensory circuits in the lateral line system of zebrafish. The evidence supporting the claims of the authors is **solid**, although further work directly testing the roles of different sema7a isoforms would strengthen the analysis. The work will be of interest to developmental neuroscientists studying circuit formation.

https://doi.org/10.7554/eLife.89926.1.sa4

Abstract

In a developing nervous system, axonal arbors often undergo complex rearrangements before neural circuits attain their final innervation topology. In the lateral line sensory system of the zebrafish, developing sensory axons reorganize their terminal arborization patterns to establish precise neural microcircuits around the mechanosensory hair cells. However, a quantitative understanding of the changes in the sensory arbor morphology and the regulators behind the microcircuit assembly remain enigmatic. Here, we report that Semaphorin7A (Sema7A) acts as an important mediator of these processes. Utilizing a semi-automated three-dimensional neurite tracing methodology and computational techniques, we have identified and quantitatively analyzed distinct topological features that shape the network in wild-type and Sema7A loss-of-function mutants. In contrast to those of wild-type animals, the sensory axons in Sema7A mutants display aberrant arborizations with disorganized network topology and diminished contacts to hair cells. Moreover, ectopic expression of a secreted form of Sema7A by non-hair cells induces chemotropic guidance of sensory axons. Our findings demonstrate that Sema7A functions both as a juxtracrine and as a secreted cue to pattern neural circuitry during sensory organ development.

Introduction

Pathfinding axons are directed to their appropriate synaptic targets by a variety of guidance cues. While approaching or traversing the target field, the growth cones of migrating axons encounter secreted or cell surface-attached ligands and respond by steering toward or away from their sources (1–4). Fine-grained control of these factors is critical for the establishment of proper neural circuitry.

The zebrafish's lateral line provides a tractable *in vivo* system for exploring the mechanisms that guide the assembly of neural circuits in a peripheral nervous system. In particular, it is possible to detect individual hair cells and the sensory axons that innervate them throughout the first week of development (5). The primary posterior lateral line on each side of the zebrafish's tail consists of about seven neuromasts, which contain mechanoreceptive hair cells of opposing polarities—half sensitive to headward (rostrad) water motion and the complementary half to tailward (caudad) water motion—that cluster at their centers (6). The sensory axons of the lateral-line nerve branch, arborize, and consolidate around the basolateral surfaces of the hair cells (**Figure 1A**). To aid in an animal's swimming behavior, these hair cells sense water currents and relay signals to the brain through the sensory axons (7). The well-defined structure of the ramifications and synaptic contacts of the sensory axons highlight the need to determine the molecular signals behind the assembly of such precise microcircuits (8). We adopted a candidate-gene strategy to seek factors that direct the growth of afferent growth cones in the zebrafish's lateral line. Analysis of single-cell RNA sequencing data identified the *semaphorin7a* (*sema7a*) gene to be highly expressed in hair cells of that organ (9). Semaphorins are important regulators of axonal growth and target finding during the patterning of diverse neural circuits (10). The semaphorin family includes proteins that are secreted, transmembrane, and cell surface-attached (11). Among these, Semaphorin7A (Sema7A) is the only molecule that is anchored to the outer leaflet of the lipid bilayer of the cell membrane by a glycosylphosphatidylinositol (GPI) linker (11). Unlike many other semaphorins, which act as repulsive cues (12,13), Sema7A is involved in promoting axon growth (4) and imparting directional signals by interacting with the integrin and plexin families of receptors residing on the pathfinding axons (14–16). Sema7A likely occurs *in vivo* in both GPI-anchored and soluble forms (17–19), and studies of neuronal explants confirm that both forms can induce directed axonal outgrowth (4). Furthermore, it has been proposed that the GPI anchor is cleaved by membrane-resident GPI-specific phospholipases (GPI-PLs) or matrix metalloproteases to release the Sema7A into the extracellular environment and thus regulate dynamic cellular processes (20,21). Because these observations indicate that Sema7A might influence neuronal development both as a juxtracrine and as a diffusive signal, we investigated the role of Sema7A in sculpting a vertebrate peripheral sensory organ.

Results

Sema7A expression and localization in hair cells

The zebrafish genome contains a single *sema7a* gene that produces two transcripts. One transcript encodes Sema7A-GPI, a full-length, GPI-linked, cell surface-attached protein. The second transcript yields Sema7A^{sec}, a protein with a truncated C-terminus, which we conjecture is secreted into the local environment. Each transcript encodes an N-terminal signal sequence and a single copy of the conserved sema domain (11). Using primers that flank the regions encoding the sema domain and the distinct C-termini of the two transcripts, we performed reverse transcription and polymerase chain reactions (RT-PCR) to identify both the membrane-anchored and the secreted

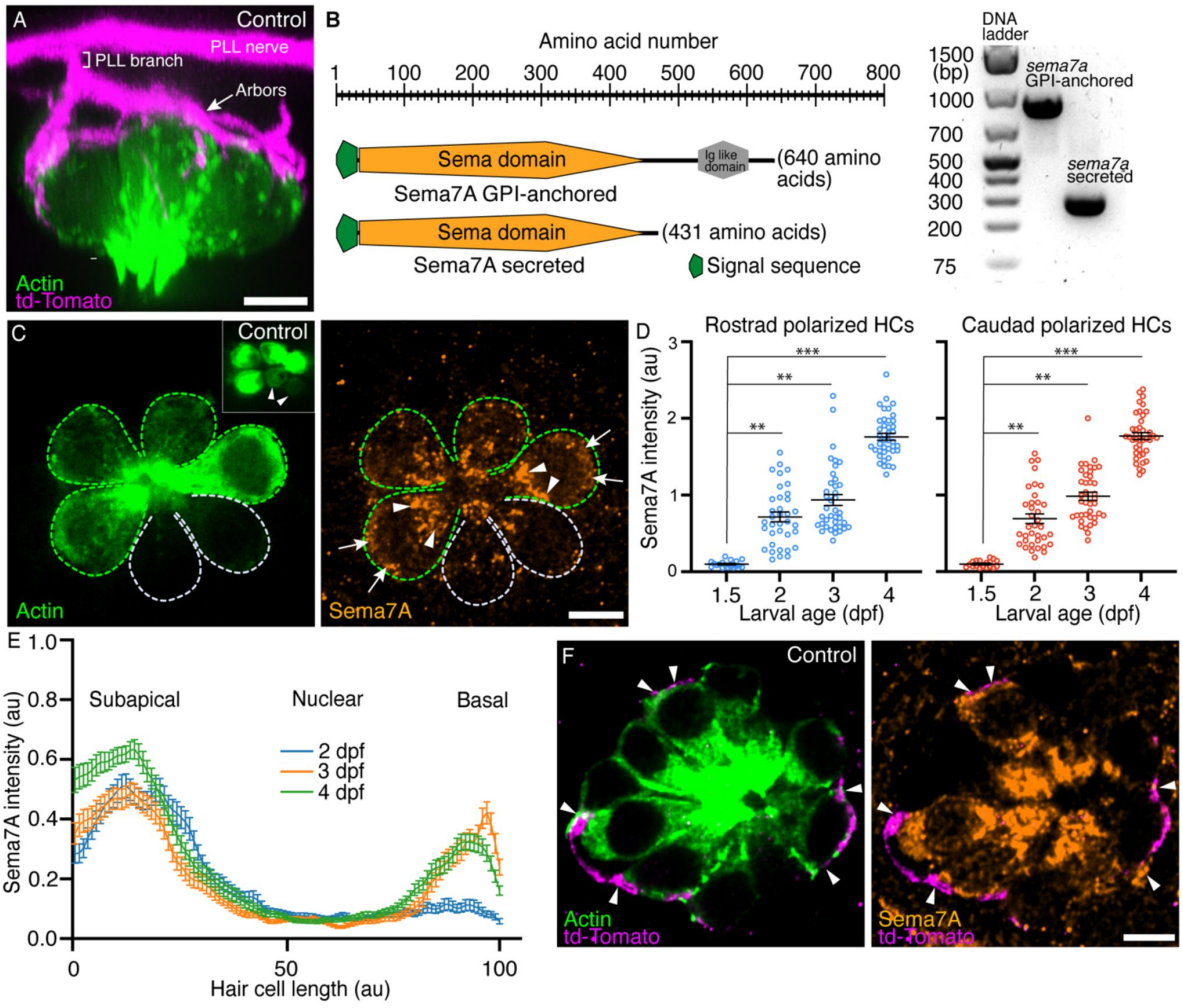

Figure 1.

Expression of Semaphorin7A in the zebrafish's lateral line.

(A) A volumetric rendering of a PLL neuromast depicts the sensory axons (magenta) that branch from the lateral line nerve to arborize around the basolateral surface of the hair cell cluster (green). Additional cell types in the neuromast are not labeled. Larval age, 3 dpf. (B) A schematic drawing of the two variants of the Sema7A protein molecule depicts the full-length GPI-anchored form and the smaller, potentially secreted form. Both the molecules include a signal sequence (green) and a conserved sema domain (orange). Gel-based RT-PCR analysis indicates the presence of both the variants in developing larva. (C) A surface micrograph of a neuromast at 3 dpf depicts two pairs of mature hair cells (green dashed lines) and a pair of immature hair cells (grey dashed lines). Inset: among the three pairs of hair cell apices, the immature pair is indicated by arrowheads. Immunolabeling reveals that the Sema7A protein (orange) occurs consistently at the subapical region (arrowheads) and at the basolateral surface (arrows) of a hair cell. In this and in each of the subsequent neuromast images, anterior is to the left and dorsal to the top. (D) A plot quantifies developmental changes in the average Sema7A intensity in both rostrally and caudally polarized hair cells of neuromasts from 1.5 dpf to 4 dpf. The data stem from 18, 36, 39, and 40 hair cells in neuromasts of respectively 1.5 dpf, 2 dpf, 3 dpf, and 4 dpf larvae. (E) A plot quantifies the distribution of average Sema7A intensity along the hair cell's apicobasal axis. The results stem from 52, 57, and 54 hair cells of neuromasts from 2 dpf, 3 dpf, and 4 dpf larvae. (F) An immunofluorescence image at the nuclear level of a 4 dpf neuromast shows the contact of the sensory arbors (magenta) with the basolateral surface of the hair cells (green). Immunolabeling for Sema7A (orange) reveals enrichment of the protein at the hair cell bases and sensory-axon interfaces (arrowheads). HC, hair cell; Scale bars, 5 μm; au, arbitrary unit; means ± SEMs; *** implies $p < 0.001$.

transcript in developing larvae (**Figure 1B**; **Figure 1—figure supplement 1A**). Single-cell RNA sequencing data also have shown that the *sema7a* transcript is particularly enriched in the immature and mature hair cells of the neuromast during early larval development (9), a period when sensory axons of the posterior lateral line contact hair cells and form synapses with them (5,22). Indeed, we have observed Sema7A to be specifically localized in both mature and immature hair cells (**Figure 1C**; **Figure 1—figure supplement 1B-E**).

As neuromasts mature, the contacts between sensory axons and hair cells increase in number, become stabilized, and establish synapses (5,22). Because Sema7A can modulate axon guidance (4,14) and synapse formation (15), we wondered whether the level of Sema7A also changes during neuromast development. Upon quantifying the average intensity of Sema7A, we found similar expression in rostrally and caudally polarized hair cells of neuromasts at 1.5, 2, 3, and 4 days post fertilization (dpf). The average Sema7A intensity increased significantly over this period in both rostrally and caudally polarized hair cells. At 1.5 dpf, the neuromasts harbor primarily immature hair cells that make minimal contacts with sensory axons and do not form stable association with axonal terminals (22). At this stage the average Sema7A intensity in hair cells remained low. By 2-4 dpf the hair cells mature to form stable contacts and well-defined synapses with the sensory axons (5,23). The average Sema7A intensity in hair cells at each of these stages rose to levels that significantly exceeded those of 1.5 dpf neuromasts (**Figure 1D**). This rise in the amount of Sema7A during neuromast maturation supports a role for Sema7A in the guidance of sensory axons and their interaction with hair cells.

We additionally demonstrated an anisotropic distribution of Sema7A along the apicobasal axis of each hair cell. As neuromasts develop through 2, 3, and 4 dpf, Sema7A remained highly enriched in the subapical region of the hair cell, the site of the Golgi network. This localization suggests that Sema7A—like other proteins of the semaphorin family (24)—is directed to the plasmalemma through Golgi-mediated vesicular trafficking. While Sema7A maintained a high level in the subapical region, the protein increasingly accumulated at the base of the hair cell: the Sema7A level at the hair cell base was low at 2 dpf, but increased sharply by 3 dpf and 4 dpf (**Figure 1E**; **Figure 1—figure supplement 1F**, **G**). During this period the hair cells increase in number and mature, whereas the associated sensory axons arborize to contact multiple hair cells and form robust synaptic boutons at their bases (5,23). The progressive enrichment of Sema7A at the hair cell base and sensory-axon interface (**Figure 1E**, **F**; Video 1) suggests that Sema7A acts as a mediator of contacts between sensory axons and hair cells.

Sema7A restricts sensory axons around clustered hair cells

If Sema7A guides and restricts the sensory arbors at and around the hair cells clustered in a neuromast, then inactivating Sema7A function should disrupt this process. To test this hypothesis, we obtained a *sema7a* mutant allele (*sema7a*^{sa24691}) with a point mutation that introduces a premature stop codon in the conserved sema domain (**Figure 2—figure supplement 1A**). The homozygous mutant, hereafter designated *sema7a*$^{-/-}$, should lack both the secreted and the membrane-attached forms of Sema7A. The average intensity of Sema7A immunolabeling in hair cells diminished by 61% in *sema7a*$^{-/-}$larvae (0.34 ± 0.01 arbitrary units) in comparison to controls (0.87 ± 0.01 arbitrary units). In a few cases we observed minute accumulations of Sema7A at the subapical region, but little or no protein at the base of the mutant hair cells (**Figure 2A**; **Figure 2—figure supplement 1B**).

To characterize the impact of the *sema7a*$^{-/-}$ mutation on arbor patterning, we utilized doubly labeled transgenic fish *Tg(myo6b:actb1-EGFP;neurod1:tdTomato)* that marked the hair cells and the sensory axons of the posterior lateral line with distinct fluorophores (25). In control neuromasts, the sensory axons approached, arborized, and consolidated around the bases of clustered hair cells (**Figure 2B**). Although the sensory axons approached the hair cells of *sema7a*$^{-/-}$ neuromasts, they displayed aberrant arborization patterns with wayward projections that extended transversely to the organ (**Figure 2C**). To quantitatively analyze the arborization

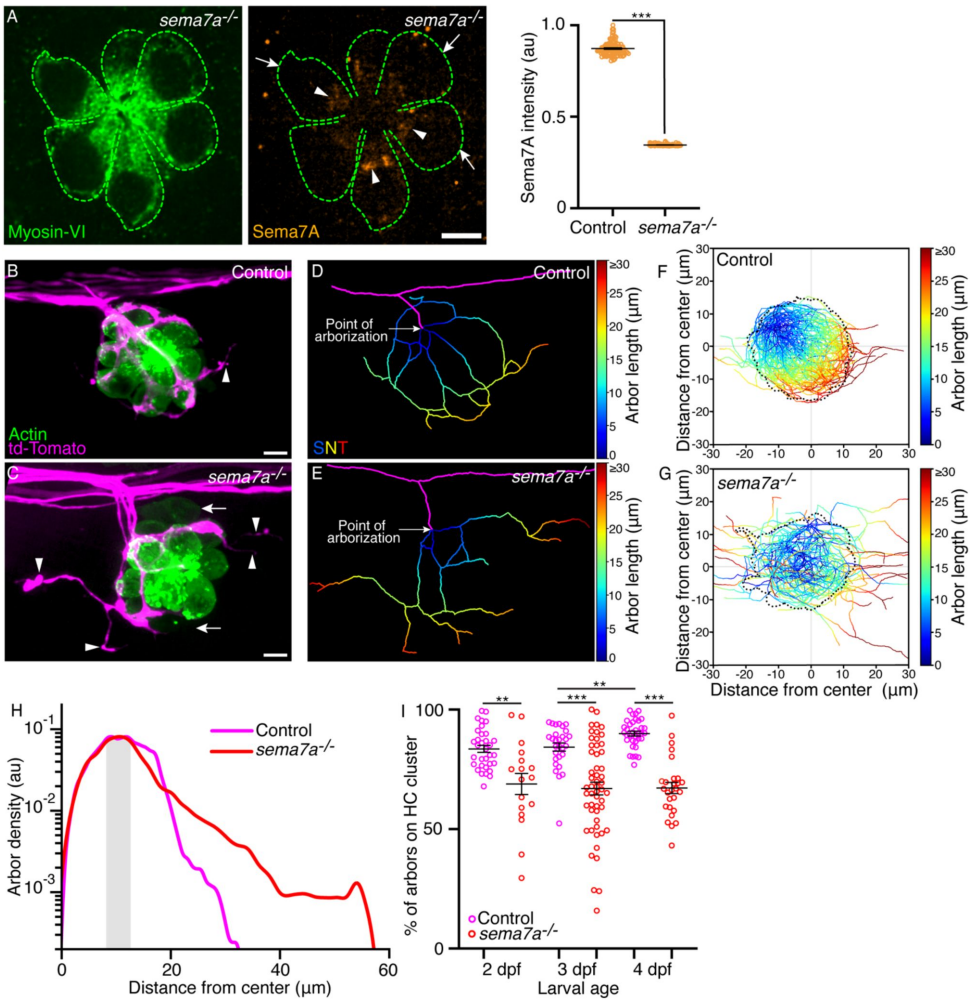

Figure 2.

sema7a$^{-/-}$ mutants display aberrant sensory axon arborizations.

(A) In a micrograph of a 3 dpf *sema7a*$^{-/-}$ neuromast, Myosin VI (green) marks the hair cells (green dashed lines) in which the level of Sema7A (orange) is highly reduced, with sporadic localization in the subapical region (arrowheads) and none in the basolateral (arrow) region. A plot of normalized Sema7A intensity from 99 control and 100 *sema7a*$^{-/-}$ hair cells quantitates the effect. (B,C) Surface views of a control and a *sema7a*$^{-/-}$ neuromast at 4 dpf depict the interaction of the sensory arbors (magenta) with hair cell clusters (green). In the control, the arbors intimately contact the hair cells, with a few exceptions (arrowhead). In the *sema7a*$^{-/-}$ mutant, the arbors direct many aberrant projections (arrowheads) away from the hair cell cluster. The two immature hair cell pairs in the *sema7a*$^{-/-}$ neuromast are indicated by arrows. (D,E) Skeletonized networks portray the three-dimensional topology of the sensory arbors from the control and the *sema7a*$^{-/-}$ neuromasts depicted in panels B and C. The pseudocolored trajectories depict the increase in arbor contour length from each point of arborization, defined as the point at which the lateral line branch (magenta) contacts hair cell cluster. (F,G) Micrographs depict the skeletonized networks of the combined 4 dpf hair cell clusters, whose centers are located at (0,0). The X- and Y-coordinates represent the anteroposterior (AP) and the dorsoventral (DV) axes of the larva, respectively. Positive values of the X- and Y-coordinates represent the posterior and ventral directions, respectively. Combined skeletonized network traces from 27 control and 27 *sema7a*$^{-/-}$ mutant neuromasts are represented. H) The plot denotes the densities of the sensory arbors around the center of the combined hair cell clusters for 35 control (magenta) and 27 *sema7a*$^{-/-}$ (red) neuromasts at 4 dpf. The shaded area marks the region proximal to the boundary of the combined hair cell cluster. (I) The plot quantifies the degree of contact of the sensory arbors to their hair cell clusters in individual neuromasts from both control (magenta) and *sema7a*$^{-/-}$ mutants (red), each point represents a single neuromast. Thirty-three, 29, and 35 neuromasts were analyzed from 2 dpf, 3 dpf, and 4 dpf control larvae, respectively. Seventeen, 53, and 27 neuromasts were analyzed from 2 dpf, 3 dpf, and 4 dpf *sema7a*$^{-/-}$ mutant larvae, respectively. HC, hair cell; Scale bars, 5 μm; au, arbitrary unit; means ± SEMs; *** signifies $p < 0.001$; ** signifies $p < 0.01$.

morphology, we traced the sensory arbors in three dimensions to generate skeletonized network traces that depict–as pseudocolored trajectories–the increase in arbor length from the point of arborization (**Figure 2D**, **E**).

To visualize the hair cell clusters and associated arborization networks from multiple neuromasts, we aligned images of hair cell clusters, registered them at their hair bundles, from neuromasts at 2 dpf, 3 dpf, and 4 dpf. Throughout development, the arborization networks of control neuromasts largely remained within the contours of the hair cell clusters; the few that reached farther nonetheless lingered nearby (**Figure 2F**). This result suggests that an attractive cue retained the axons near the sensory organ. In *sema7a*$^{-/-}$ neuromasts, however the neuronal arbors failed to consolidate within the boundaries of hair cell clusters and extended far beyond them (**Figure 2G**; **Figure 2—figure supplement 1C-H**; Video 2).

We quantified the distribution of the sensory arbors around the center of the combined hair cell clusters. For both the control and the *sema7a*$^{-/-}$ neuromasts, the arbor densities peaked proximal to the boundaries of the hair cell clusters. Beyond the cluster boundaries, in control neuromasts at 2 dpf, 3 dpf, and 4 dpf the arbor densities fell sharply at respectively 31.7 μm, 36.6 μm, and 32.7 μm from the center. In *sema7a*$^{-/-}$ neuromasts of the same ages, the sensory arbors extended respectively 38.5 μm, 51.4 μm, and 56.6 μm from the center (**Figure 2H**; **Figure 2—figure supplement 1I**, **J**; **Figure 2—figure supplement 2A**). Furthermore, we quantified the degree of contact of the sensory arbors to their hair cell clusters in individual neuromasts from both control and *sema7a*$^{-/-}$mutants. In control neuromasts, the degree of contact was 83 ± 1 % (mean ± SEM) at 2 dpf and 84 ± 1 % at 3 dpf, but significantly increased to 90 ± 1 % at 4 dpf (**Figure 2I**; **Figure 2—figure supplement 2B**). This observation indicates that the sensory arbors reinforce their association to the hair cell clusters as neuromasts develop. However, in *sema7a*$^{-/-}$ neuromasts such contact was significantly reduced. Only 69 ± 4 % of sensory arbors at 2 dpf were closely associated with the corresponding hair cell clusters, a value that remained at 67 ± 2 % at both 3 dpf and 4 dpf (**Figure 2I**). These findings signify that, with simultaneous disruption of both signaling modalities of Sema7A, the organ fails to restrict the localization of sensory arbors and has significantly diminished contact with them.

Sema7A patterns the arborization network's topology

Accurate spatial arrangement of the neuronal projections around hair cells is essential for proper retrieval and transmission of sensory information. Mutations that perturb proper assembly of sensory neuronal microcircuits lead to hearing impairment (26). Quantitative insight into the wiring pattern is therefore essential to identify systematic aberrations in the microcircuit arising from genetic deficits. The three-dimensional skeletonized network traces allowed us to accurately delineate the microcircuit topology across individuals, developmental stages, and genotypes from living animals (**Figure 2D**, **E**). To quantitatively analyze the arbor network, we defined five topological attributes: (1) nodes, denoted as junctions where arbors branch, converge, or cross; (2) loops, comprising minimal arbor cycles forming topological holes; (3) bare terminals, defined as arbors with free ends; (4) the node degree, calculated as the number of first-neighbor nodes incident to a node; and (5) the arbor curvature, measured as the total curvature of a bare terminal (**Figure 3A**). We quantified these attributes to accurately determine how the circuit topology is established during maturation of the sensory organ in control larvae and how it is impacted by *sema7a* deficit.

To determine how internode connectivity is distributed across networks, we quantified the distribution of node degrees along the relative height of the hair cell cluster across individuals, developmental stages, and genotypes. As for most other real-world networks (27), we observed a highly skewed node-degree distribution: the majority of nodes had low node degrees (three and four) and a small number of nodes—often acting as hubs, like the arborization initiation point—had high node degrees (five to seven). The node degree varied from three to seven in control larvae and three to six in *sema7a*$^{-/-}$ larvae. Across developmental stages and genotypes, the high

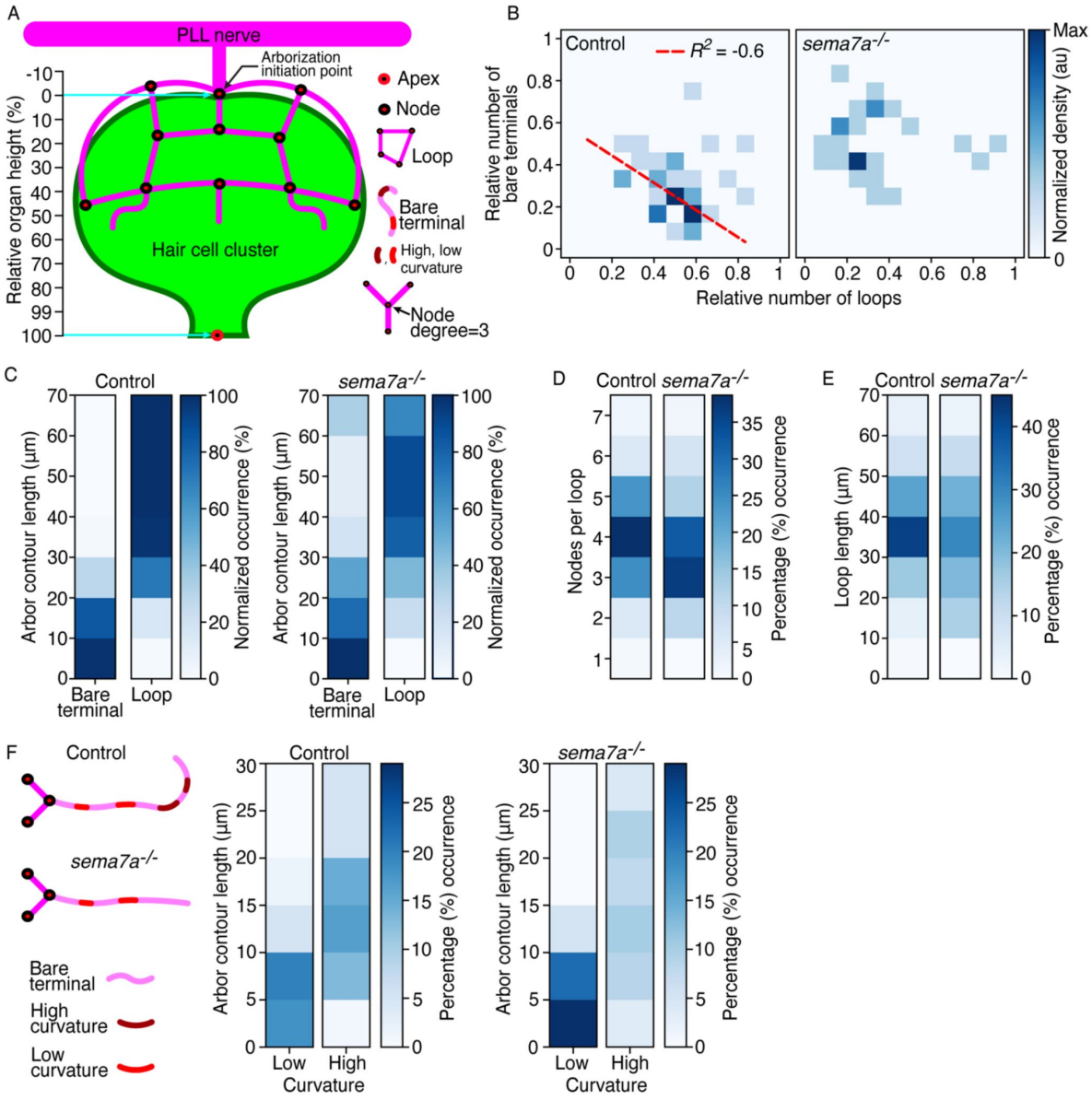

Figure 3.

Sema7A patterns the topology of the sensory arbor network .

(A) A schematic drawing of the combined hair cell cluster (green) and associated sensory axons (magenta) shows diverse topological features of the arborization network, including nodes, loops, bare terminals, node degree, and bare-terminal curvature. The apex is defined as the center of the hair bundle cluster and the base is denoted by the node from which the arborizations extends. The relative organ height describes the position along the axis formed between the arborization initiation point and the apex of the hair cell cluster. (B) The correlation between the relative number of bare terminals and loops from 35 control neuromasts and 27 *sema7a*$^{-/-}$ neuromasts at 4 dpf shows a negative correlation in the control but a scattered distribution in the mutants. The same neuromasts were analyzed in the subsequent panels. R^2, correlation coefficient. Dashed red line depicts the regression slope. (C) The relationship of contour lengths to bare terminals and loops reveals reduced looping in the mutants. (D) Quantification of the number of nodes per loop demonstrates a decrease in mutants. (E) Mutants in the same larvae manifest a broader distribution of loop lengths. (F) A schematic diagram of the extending bare terminals depicts regions of high and low curvature along the length of the arbor. The distributions of bare terminals between low-and high-curvature groups show an enrichment of long, highly curved arbors in the control and short, linear arbors in the mutants. Statistical analyses are displayed in **Table 1**.

node degrees primarily occurred at the base (region from 0 % to 10 % of the cluster height) of the hair cell cluster and acted as hubs for the majority of branching events. Low node degrees primarily occurred along the basolateral region (region from 10 % to 60 % of the cluster height) of the hair cell cluster. The apical region (region from 60 % to 100 % of the cluster height) was sparsely populated with low node degrees. The network's hierarchical organization along the organ's axis suggests that arbors receive sensory inputs at multiple levels, allowing the network to carry out robust neural computations. Even though nodes of low degree were most prevalent between genotypes across developmental stages, their distribution along the relative organ axis became significantly different at 4 dpf, with nodes in control larvae localized higher along the axis than in *sema7a*$^{-/-}$ larvae (**Figure 3A**; **Figure 3—figure supplement 1A-C**; **Table 1**). These observations indicate that Sema7A regulates both the spatial organization and node-degree complexity of the sensory arbor network.

An average of 9.3 sensory axonal branches approach the hair cell cluster of a neuromast (8). Pathfinding of sensory axons around the hair cell cluster results in the formation of axonal fascicles that form numerous loops and bare terminals, which determine the microcircuit topology (**Figure 2B**, **D**) (8). To optimally surround and contact the hair cell cluster, do the sensory arbors prefer to adopt one topological feature over the other? To address this question, we measured the correlation between the number of bare terminals and the number of loops across individuals, developmental stages, and genotypes. In both 2 dpf and 3 dpf larvae, the distributions remained highly scattered across individuals and genotypes. However, by 4 dpf in the control larvae the arbor network contained either a high number of loops with a low number of bare terminals or a high number of bare terminals with a low number of loops. This result suggests that the stereotypical circuit topology observed in the mature organ emerges from distinct events in which individual arbors transition from forming bare terminals to forming closed loops encircling topological holes. That we did not observe a similar transition in *sema7a*$^{-/-}$ neuromasts of the same age suggests that Sema7A regulates the switch between these two distinct topological features (**Figure 3B**; **Figure 3—figure supplement 1D**, **E**; **Table 1**).

Measurement of the contour length of both bare terminals and loops additionally revealed that across developmental stages in control larvae the sensory arbors followed a three-step process to choose the appropriate topological feature: arbors shorter than 10 μm always formed bare terminals; arbors between 10 μm and 30 μm began to switch between features, with arbors longer than 20 μm strongly preferring to form loops; and arbors longer than 30 μm always formed loops. These results imply that the switch between bare terminals and loops is partly dependent on the length of the arbors. However, this characteristic topological preference was significantly perturbed in the *sema7a*$^{-/-}$ larvae across developmental stages, as many of the sensory arbors longer than 30 μm remained as bare terminals (**Figure 3C**; **Figure 3—figure supplement 1F**, **G**; **Table 1**). Furthermore, in 4 dpf control neuromasts the majority of the loops contained four nodes and utilized 30-40 μm of arbors to form closed cycles. These conserved topological attributes were significantly perturbed in the *sema7a*$^{-/-}$larvae of same age (**Figure 3D**, **E**; **Figure 3—figure supplement 2A-D**; **Table 1**). These findings indicate that Sema7A tightly regulates the sensory arbor loop formation, including the preferred loop length and number of nodes per loop, to properly surround and contact the hair cell cluster.

As observed previously, bare terminals in control neuromasts project transverse to the organ and linger nearby, often curving back to form new loops and contact the hair cell cluster (**Figure 2D**, **F**). To analyze the propensity of the bare terminals to curl backward, we measured their total curvatures, defined as the sum of the curvature at each point along the length of an arbor. Henceforth, we address the total curvature as the curvature of a bare terminal. We classified the bare terminals in two categories: high-curvature arbors with curled morphology and curvature greater than $\pi/6$ (30 degrees); and low-curvature arbors with linear morphology and curvature less than π /6. In control neuromasts 44.8 % of arbors had low curvature compared to 56.4 % in *sema7a*$^{-/-}$ neuromasts at 4 dpf. Concomitantly, 55.2 % of arbors had high curvature in control

Height of node degrees	*p*-values (control vs *sema7a*$^{-/-}$)		
	2 dpf	3 dpf	4 dpf
Degree = 3	3.50E-01	1.05E-08*	1.68E-03*
Degree = 4	3.85E-01	7.11E-02	1.71E-03*
Degree = 5	4.60E-01	5.23E-01	4.40E-01
Bare terminals vs Loop	2 dpf	3 dpf	4 dpf
0 to 10 μm	3.84E-01	7.89E-01	2.11E-01
10 to 20 μm	3.50E-02*	3.92E-01	2.94E-02*
20 to 30 μm	2.28E-04*	2.63E-02*	3.82E-09*
30 to 40 μm	5.04E-59*	3.63E-25*	1.28E-33*
40 to 70 μm	———	———	———
Nodes per loop	5.06E-01	1.96E-01	3.50E-02*
Loop length	5.81E-01	2.71E-01	2.21E-02*
Distribution of bare terminal curvature	2 dpf	3 dpf	4 dpf
	4.23E-01	8.91E-01	1.99E-02*

Table 1.

Statistical comparison between control and *sema7a*$^{-/-}$ larvae for topological features.

One-sided Kolmogorov-Smirnov tests were used to assess the difference in node degree heights, nodes per loop, and loop lengths for control *versus sema7a*$^{-/-}$ neuromasts at 2 dpf, 3 dpf, and 4 dpf. In each of these cases, the difference in the distributions were not significantly different (*p*-values in red) between the control and the mutants at 2 dpf and 3 dpf but became significantly different (*p*-values in green) at 4 dpf. Chi-square tests were used to assess the difference in occurrences of bare terminals *versus* loops, as well as the occurrences of bare terminals with low *versus* high curvature. The distribution at 4 dpf shows significant difference between the control and the mutant larvae. The occurrence of significant differences at 4 dpf for diverse topological features suggest that Sema7A function is required to achieve an ordered network topology at a mature stage. Thirty-three, 29, and 35 neuromasts were analyzed from 2 dpf, 3 dpf, and 4 dpf control larvae, respectively, and 17, 53, and 27 neuromasts were analyzed from 2 dpf, 3 dpf, and 4 dpf *sema7a*$^{-/-}$ mutant larvae, respectively. * signifies $p < 0.05$.

neuromasts compared to 43.6 % in *sema7a*$^{-/-}$ neuromasts at 4 dpf (**Figure 3F**; **Figure 3—figure supplement 2E**, **F**; **Table 1**). These observations further confirm our hypothesis that a Sema7A-mediated attractive cue is involved in orienting bare neural arbors toward the hair cell cluster to potentially form loops.

In summary, we propose that Sema7A regulates four key aspects of the topology of the arborization network: (1) the node degree complexity along the organ's axis; (2) the transition of arbors from bare terminals to loops; (3) the preference for forming loops containing four nodes with 30-40 µm of arbors; and (4) the preference of bare terminals to adopt higher curvature.

Sema7A^{sec} is a sufficient chemoattractive cue for sensory axon guidance

Because genetic inactivation of the *sema7a* gene disrupts both signaling modalities of the cognate protein, we could not assess the specific activity of the Sema7A^{sec} diffusive cue in guiding lateral-line sensory axons. To independently verify the potential role of that isoform, we therefore expressed the secreted variant ectopically and investigated the resultant arborization patterns.

Analysis of the microcircuit connectivity of the neuromasts has demonstrated bare sensory-axonal terminals in the perisynaptic compartments, where they do not contact the hair cell membrane (8). We speculate that these bare terminals are attracted by a Sema7A^{sec} diffusive cue. To test this hypothesis, we ectopically expressed Sema7A^{sec} protein tagged with the fluorophore mKate2, then analyzed its effect on the morphology of sensory arbors. Fertilized one-cell embryos were injected with the *hsp70:sema7a^{sec}-mKate2* plasmid and raised to 3 dpf. Larvae expressing the transgenesis marker—the lens-specific red fluorescent protein mCherry—were heat-shocked, incubated to allow expression, and subsequently mounted for live imaging. In these larvae, a random mosaic of cells—often embryonic muscle progenitors in the dermomyotome or mature myofibers—expressed the exogenous Sema7A^{sec}-mKate2 protein. We selected only those neuromasts in which an ectopic integration had occurred near the network of sensory arbors (**Figure 4A,B**). In all 22 such cases, we observed robust axonal projections from the sensory arbor network toward the ectopically expressing Sema7A^{sec} cells. When the exogenous *sema7a^{sec}* integration occurred in embryonic muscle progenitor cells, which reside in a superficial layer external to the muscle fibers and adjacent to the larval skin (28), the projections were able to form direct contacts with them (**Figure 4C**; Videos 3, 4). But more often, when mature myofibers expressed the exogenous Sema7A^{sec} deep in the myotome, the axonal projections approached those targets but failed to contact them (**Figure 4D**, Videos 5, 6). This behavior likely arose because other components in the myotomal niche—including the fibrous epimysium, other myofibers, myoblasts, and immature myotubes whose surroundings are permeable to diverse diffusive cues (29)—physically obstructed direct interaction of the extended neurites with the ectopically expressing myofibers. All 18 of the injected but not heat-shocked control larvae did not express ectopic Sema7A^{sec}, and we did not observe aberrant projections from the sensory arbor network (**Figure 4E**).

To measure the accuracy of the extended axonal projections in finding the ectopic Sema7A^{sec} source, we defined three parameters: (1) the source path, denoted as the linear distance from the point of arborization to the boundary of an ectopically expressing Sema7A^{sec} cell; (2) the projection path, representing the linear distance from the point of arborization to the terminus of the extended projection; and (3) the projection proximity, calculated as the linear distance from the terminus of the extended axonal projection to the nearest boundary of the ectopically expressing Sema7A^{sec} cell (**Figure 4B**). We quantified these parameters from 18 of the 22 mosaic integration events; in the remainder the extended axonal projections– although following the ectopic source–reentered the posterior lateral-line nerve so that identification of the axon terminals was not possible (**Figure 4—figure supplement 1A-A**"; Video 7). When we plotted the

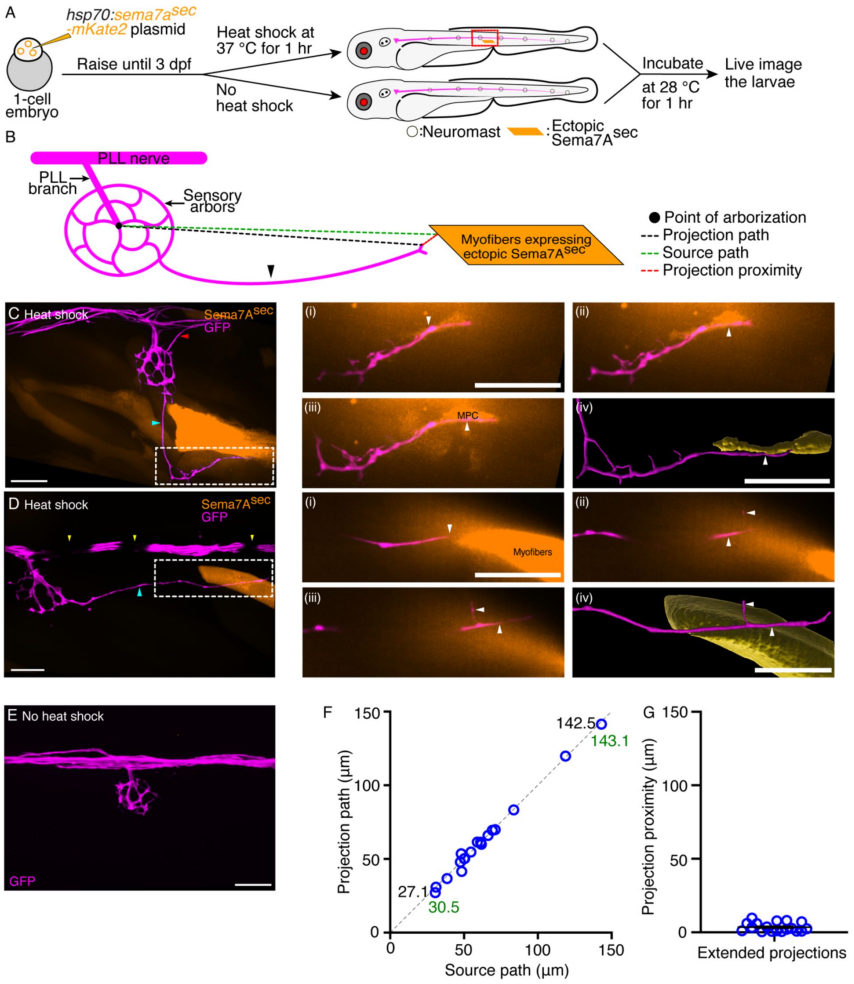

Figure 4.

Ectopic Sema7A^{sec} diffusive cue provides neural guidance *in vivo*.

(A) A diagrammatic overview depicts the generation of a transgenic animal that expresses the Sema7A^{sec} protein ectopically under the control of a thermally inducible promoter. Larvae with ectopic myotomal-integration near the network of sensory arbors (red line) were imaged to analyze arbor morphology. (B) A schematic drawing of a sensory arbor from a heat-shocked larva depicts an extended axonal projection (arrowhead) that reaches toward the myofibers expressing the ectopic Sema7A^{sec} protein. Parameters that quantitate the accuracy of the extended axonal projections toward the ectopic Sema7A^{sec} sources are denoted. (C) In a micrograph of an ectopically expressing Sema7A^{sec} (orange) larva, the sensory arbor (magenta) extends two aberrant axonal projections. One elongates (cyan arrowhead) along the somite boundary to reach and contact an ectopically integrated muscle progenitor cell (white dashed line) and the other (red arrowhead) reenters the posterior lateral-line nerve while following a second ectopic source. The through-focus scans (i–iii) from the epidermis to the dermomyotome and the three-dimensional (3D) surface reconstruction (iv) reveal the intimate contact between the aberrant sensory arbor (arrowheads) and the muscle progenitor cell. (D) In a micrograph of an ectopically expressing Sema7A^{sec} (orange) larva, the sensory arbor (magenta) extends a single aberrant axonal process (cyan arrowhead) to reach ectopically integrated myofibers (white dashed line). The through-focus scans (i–iii) from the epidermis to the dermomyotome and the 3D surface reconstruction (iv) reveal the proximal association of the aberrant sensory arbor (arrowheads) to the myofibers. Melanocytes (yellow arrowhead) along the horizontal myoseptum intermittently block the visibility of the lateral-line nerve. (E) An injected, but not heat-shocked, control larva does not express ectopic Sema7A^{sec} and does not show aberrant projection from the sensory arbor. (F) A plot demonstrates the accuracy of 18 extended axonal arbors in finding ectopic Sema7A^{sec} sources. Each circle represents a single ectopic integration event. The two pairs of numbers represent the minimal and maximal lengths of the projection path (black) and its corresponding source path (green). (G) A plot quantitates the distribution of projection-proximity length from 18 ectopic integration events. MPC, muscle progenitor cell; scale bars, 20 µm; means ± SEMs.

projection path length against the source-path length, we observed a nearly perfect correlation (**Figure 4F**). This result signifies that irrespective of the location of the ectopic source–whether proximal or distal to the sensory arbor network–the Sema7A^{sec} cue sufficed to attract axonal terminals from the sensory arbor. Furthermore, the low average projection-proximity length of 3.5 ± 0.7 µm (mean ± SEM) indicated that the extended projection terminals remained either in contact (8 of 18) or in the vicinity (10 of 18) of the ectopic Sema7A^{sec} sources (**Figure 4G**). These observations together demonstrate that the Sema7A^{sec} diffusive cue is sufficient to provide neural guidance *in vivo*.

As the posterior lateral-line ganglion matures, newly formed neurons extend their axonal growth cones along the posterior lateral-line nerve to reach the neuromasts (30). We wondered whether the axonal projections that had yet to be associated with a neuromast could also respond to an ectopic source of Sema7A^{sec}. Indeed, on five occasions in which *sema7a^{sec}* integration had occurred between two neuromasts, we detected neurite extensions from the posterior lateral-line nerve to the ectopic Sema7A^{sec} source (**Figure 4—figure supplement 1B-B**"; Videos 8-10). The responsiveness of the posterior lateral-line axons to Sema7A^{sec} might therefore be an intrinsic property of the neurons that does not require the neuromast microenvironment.

Sema7A deficiency impacts synaptic assembly

Contact stabilization between an axon and its target cell is essential for synapse formation (31). Neural GPI-anchored proteins can act as regulators of various synaptic-adhesion pathways (32). In the mouse olfactory system, GPI-anchored Sema7A is enriched in olfactory sensory axons and mediates sustained interaction with the dendrites of mitral and tufted cells in the olfactory bulb to establish synapses (15). In the developing mouse brain–particularly in Purkinje cells–GPI-anchored Sema7A instead regulates the elimination of synapses onto climbing fibers (33). The role of anchored Sema7A in regulating synaptic architecture can thus vary according to the cell type and developmental stage. Our demonstration that Sema7A is necessary to consolidate the contact between sensory axons and hair cells during neuromast development suggests a possible role in regulating synaptic structure.

Proper synaptogenesis requires the correct spatial organization of the presynaptic and postsynaptic apparatus at the apposition of two cells. At the interface between hair cells and sensory axons, the synaptic network involves two scaffolding proteins in particular: ribeye, a major constituent of the presynaptic ribbons (34), and membrane-associated guanylate kinase (MAGUK), a conserved group of proteins that organize postsynaptic densities (35). Utilizing these scaffolding proteins as markers, we investigated the impact of the *sema7a$^{-/-}$* mutation on synapse formation. To analyze the distribution of presynaptic densities–immunolabeled with an antibody against the ribeye-associated presynaptic constituent C-terminal binding protein (CTBP) (34)–we counted the number and measured the area of CTBP punctae from multiple neuromasts at several stages of neuromast development (**Figure 5A**, **B**). The CTBP punctae in each hair cell ranged from zero to seven across developmental stages. In the zebrafish's posterior lateral line, the formation of presynaptic ribbons is an intrinsic property of the hair cells that does not require contact with lateral-line sensory axons. However, sustained contact with the sensory axon influences the maintenance and stability of ribbons (36). As neuromasts matured from 2 dpf to 4 dpf, we identified similar distribution patterns with a characteristic increase in the number of CTBP punctae in both control and *sema7a$^{-/-}$*larvae (**Figure 5C**, **D**). This result implies that the formation of new presynaptic ribbons is not perturbed in the mutants, even though there are on average fewer CTBP punctae (**Figure 5—figure supplement 1A-C**). Measurement of the areas of CTBP punctae also showed similar distributions in both genotypes (**Figure 5E**, F) but the average area of presynaptic densities was reduced in the mutants (**Figure 5—figure supplement 1D-F**).

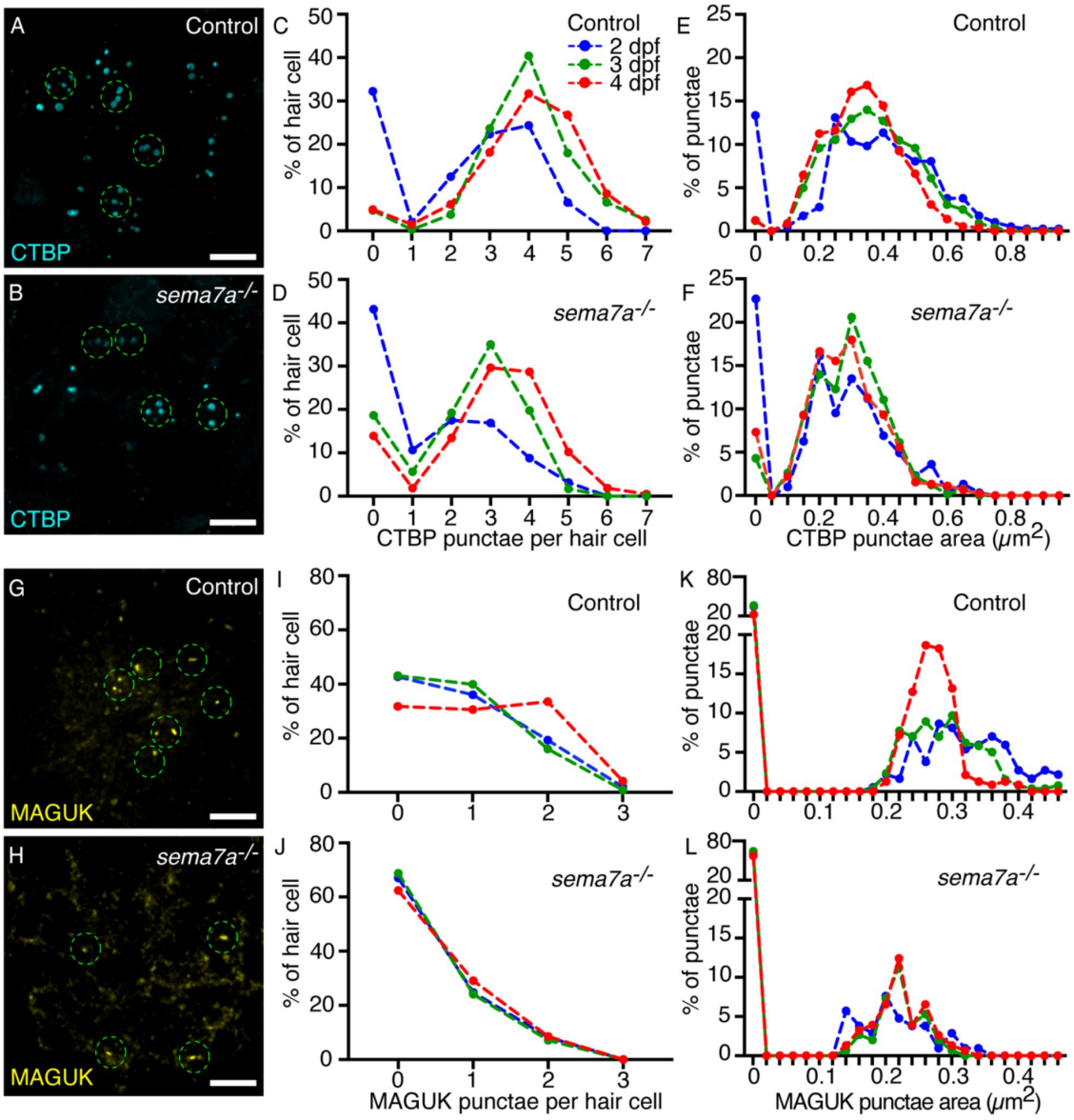

Figure 5.

Sema7A deficiency impairs synaptic assembly.

(A,B) Maximal-intensity projections of micrographs from a control and a *sema7a*$^{-/-}$ neuromast depict the presynaptic aggregates marked by CTBP (cyan). The approximate hair cell basal region is outlined by dashed green circles. (C-F) Plots quantitate the numbers of presynaptic aggregates (C,D) and their areas (E,F), in each hair cell across developmental stages. One hundred and fifty-two, 317, and 325 hair cells were analyzed from 2 dpf, 3 dpf, and 4 dpf control larvae, respectively. One hundred and sixty, 216, and 177 hair cells were analyzed from 2 dpf, 3 dpf, and 4 dpf *sema7a*$^{-/-}$mutant larvae, respectively. (I,J) Maximal-intensity projections from micrographs of a control and a *sema7a*$^{-/-}$ neuromast depict the postsynaptic aggregates marked by MAGUK (yellow). The approximate hair cell basal region is outlined by dashed green circles. (K-N) Plots quantitate the numbers of postsynaptic aggregates (K,L) and their areas (M,N), in each hair cell across developmental stages. One hundred and fifty, 218, and 167 hair cells were analyzed from 2 dpf, 3 dpf, and 4 dpf control larvae, respectively. Ninety-seven, 141, and 141 hair cells were analyzed from 2 dpf, 3 dpf, and 4 dpf *sema7a*$^{-/-}$ mutant larvae, respectively. Scale bars, 5 μm.

Because GPI-anchored Sema7A lacks a cytosolic domain, it is unlikely that Sema7A signaling directly induces formation of presynaptic ribbons. Instead, GPI-anchored Sema7A might induce postsynaptic assembly on the apposed neuronal membrane (15). To characterize the distribution of the postsynaptic aggregates–immunostained with a pan-MAGUK antibody– we performed analyses similar to those above (**Figure 5I**, **J**). At 4 dpf, 68.3 % of the hair cells in the control neuromasts were associated with at least one MAGUK punctum. In the *sema7a*$^{-/-}$ mutant this value fell to 37.5 % (**Figure 5K**, **L**). The average number of MAGUK punctae also declined in the mutants (**Figure 5—figure supplement 1G-I**). As control neuromasts matured from 2 dpf to 4 dpf, the MAGUK punctae showed a shift toward smaller sizes, suggesting that the postsynaptic structure fragmented into smaller entities as observed in other excitatory synapses (37). At 4 dpf, 77.5 % of the hair cells in the control neuromasts had postsynaptic densities with areas between 0.10 μm^2 and 0.40 μm^2. In the *sema7a*$^{-/-}$ mutant the corresponding value was only 42.5 % (**Fig. 4M,N**). The average area of MAGUK punctae was also reduced in the mutants compared to the controls (**Figure 5—figure supplement 1J-L**). We speculate that the abnormalities in postsynaptic structure arose from reduced contact between the hair cells and the sensory axons in the *sema7a*$^{-/-}$ mutants or from the lack of Sema7A-mediated juxtracrine signaling onto the apposed neurite terminals (15).

Discussion

The specification of neural circuitry requires precise control of the guidance cues that direct and restrict neural arbors at their target fields and facilitate synapse formation. In the lateral-line neuromast of the zebrafish, we have identified Sema7A as an essential cue that regulates the interaction between hair cells and sensory axons. We have discovered dual modes of Sema7A function *in vivo*: the chemoattractive diffusible form is sufficient to guide the sensory arbors toward their target, whereas the membrane-attached form likely participates in sculping accurate neural circuitry to facilitate contact-mediated formation and maintenance of synapses. Our results suggest a potential mechanism for hair cell innervation in which a local Sema7A^{sec} diffusive cue consolidates the sensory arbors at the hair cell cluster and the membrane-anchored Sema7A-GPI molecule regulates microcircuit topology and synapse assembly.

The role of Sema7A in regulating diverse topological features of the arborization network suggests that microcircuits of control and *sema7a*$^{-/-}$ neuromasts display important functional differences. Loss of Sema7A disrupts the hierarchical organization of the node-degree distribution along the organ's axis, as well as the preference towards forming loops containing four nodes with 30-40 μm of arbors. What benefit does the network gain from surrounding the hair cell cluster with closed loops instead of bare terminals? The network may actively form loops to contribute to the neuromast's overall structure and function, or else emerge as a consequence of the arbors navigating the intervening spaces between the hair cells and support cells. Through our ectopic expression of Sema7A^{sec}, we have observed that free spaces and physical obstructions can shape arbor morphologies, such as in the myotomal niche. However, we speculate that the precise patterning of the network—with characteristic looping behaviors—is not merely a byproduct of neuromast architecture, but rather contributes to the network's ability to perform robust neural computations and faithfully transmit sensory information to higher processing centers in the posterior lateral-line ganglion and medial octavolateralis nucleus in the hindbrain (7). Further studies are necessary to dissect the potential role of these topological features in performing robust neural computations in the lateral-line microcircuit.

Recent studies have begun to dissect the molecular mechanisms of semaphorin signaling in axonal navigation. In explants derived from the murine olfactory bulb, Sema7A interacts directly with integrinβ1 to trigger downstream signaling effectors involving focal adhesion kinase and mitogen-activated protein kinases, which are critical regulators of the cytoskeletal network during axonal pathfinding (4,38). Moreover, the interaction between Sema7A and its receptor plexinC1

activates the rac1-cdc42-PAK pathway, which alters the actin network to promote axonal guidance and synapse formation (15,39). We speculate that lateral-line sensory axons utilize similar mechanisms to sense and respond to Sema7A in the establishment of microcircuits with hair cells.

During early development of the posterior lateral line, the growth cones of sensory axons intimately associate with the prosensory primordium that deposits neuromasts along the lateral surface of the larva (40,41). The growth of the sensory fibers with the primordium is regulated by diverse neurotrophic factors expressed in the primordium (42,43). Impairing brain-derived or glial cell line-derived neurotrophic factors and their receptors perturbs directed axonal motility and innervation of hair cells (42,43). Lateral-line hair cells are particularly enriched in brain-derived neurotrophic factor (44) and other chemotropic cues (**Figure 6**). Because the sensory axons of *sema7a*$^{-/-}$ mutants reliably branch from the lateral-line nerve to reach hair cell clusters, these chemoattractive factors might compensate in part for the absence of Sema7A function. Although sensory axons are strict selectors of hair cell polarity and form synapses accordingly (5), diverse chemoattractant cues including Sema7A occur uniformly between hair cell polarities (44). It seems likely that unbiased attractive signals bring sensory arbors toward hair cells, after which polarity-specific molecules on hair cell surfaces dictate the final association between axonal terminal and hair cells. Notch-delta signaling and its downstream effectors regulate hair cell polarity and the innervation pattern (6,8,25). It would be interesting to determine whether Notch-mediated polarity signatures on the hair cell's surface can refine the neuromast neural circuitry.

Materials and Methods

Zebrafish strains and husbandry

Experiments were performed on 1.5-4 dpf zebrafish larvae in accordance with the standards of Rockefeller University's Institutional Animal Care and Use Committee. Naturally spawned and fertilized eggs were collected, cleaned, staged, and maintained at 28.5 °C in system-water with 1 µg/mL methylene blue. Wild-type AB and heterozygous mutant *semaphorin7a*^{sa24691} zebrafish were obtained from the Zebrafish International Resource Center. In addition, the following transgenic zebrafish lines were used: *Tg(myo6b:actb1-EGFP)* (45), *Tg(neurod1:tdTomato)* (25), and *TgBAC(neurod1:EGFP)* (46).

Genotyping of mutant fish

The *semaphorin7a*^{sa24691} allele harbors an A-to-T point mutation in the seventh exon of the *semaphorin7a* gene, which creates a premature stop codon (Fig. S2A). Genomic DNA was isolated from the tail fins of adult *semaphorin7a*^{sa24691}(*sema7a*^{sa91}) heterozygous mutant zebrafish. The mutant locus in the genome was PCR amplified using the following primers: sema7a^{sa91}F: 5'-AAAGCTGGAAAGCGAATCAA-3' and sema7a^{sa91}R: 5'-ATATCCAAGGATCCGCCTCT-3'. The 734-base pair amplicons were sequenced, and heterozygous adults were propagated.

Reverse transcription-polymerase chain reactions (RT PCR)

Total RNA was isolated from whole zebrafish larvae by TRIzol extraction followed by DNAse treatment (TURBO DNA-free Ambion). We used thirty 4 dpf zebrafish larvae to isolate total RNA. We generated cDNA libraries using iScript cDNA Synthesis Kit (Bio-Rad). Each transcript was PCR amplified using the following primers: sema7aF: 5'-GGTTTTTCTGAGGCCATTCC-3', sema7aR1: 5'-GGCACTCGTGACAAATGCTA-3', sema7aR2: 5'-TGTGGAGAAAGTCACAAAGCA-3' (Fig. S1A).

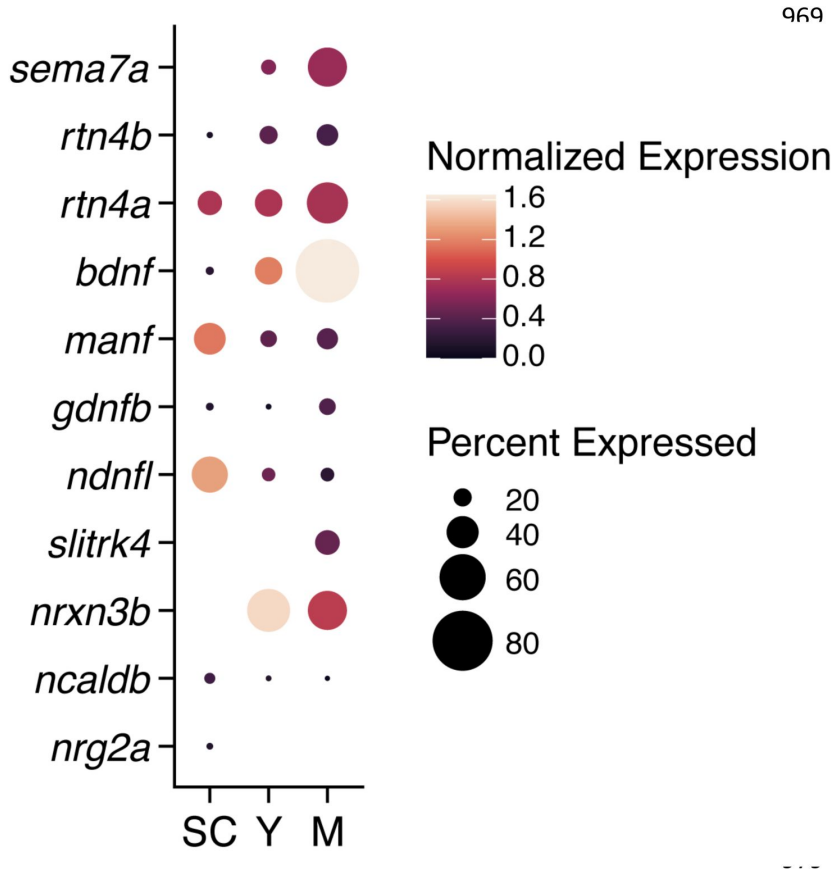

Figure 6.

Expression of diverse neural guidance cues in developing neuromasts.

Analysis of single cell RNA-sequencing data (9) shows the expression of multiple neural guidance genes that are expressed across young hair cells (Y), mature hair cells (M), and support cells (SC). Dot sizes and colors signify the proportion of cells in each cluster that express a gene and the average strength of expression (log[(counts/10,000) +1]), respectively.

Transient transgenesis with the hsp70l:sema7a^{sec}-mKate2 construct

The pDNR-LIB plasmid containing the *sema7a^{sec}* coding sequence was purchased from horizon (7140389, Perkin-Elmer). The coding sequence was PCR amplified using the following primers: sema7a^{sec}F: 5'-GGGGACAAGTTTGTACAAAAAAGCAGGCTTGATGATTCGACATTATTCT-3' and sema7a^{sec}R: 5'-GGGGACCACTTTGTACAAGAAAGCTGGGTG*CTT*TGTGGAGAAAGTCACAAAGCA-3'.

The italicized nucleotides denote the mutated stop codon. The amplicon was then cloned into the pDONR221 vector by BP recombination to generate the middle entry pME-sema7a^{sec} vector. To generate the hsp70:sema7a^{sec}-mKate2 construct, gateway cloning was performed by combining the plasmids p5E-hsp70 (47), pME-sema7a^{sec}, p3E-mKate2-myc no-pA (Addgene, 80812), and pDESTtol2pACrymCherry (Addgene, 64023) with LR Clonase II Plus (Invitrogen). Verified constructs (25 ng/µl plasmid DNA) were injected with Tol2 Transposase mRNA (approximately 25 ng/µl) into one-cell embryos. The transiently transgenic larvae— identified by the expression of red fluorescent protein (mCherry) in their lenses—were raised till 3 dpf, heat-shocked in a water bath at 37 °C for 1 hr, incubated at 28 °C for 1 hr to allow expression, and subsequently mounted for live imaging.

Microscopy and volumetric rendering of living neuronal arbors and cells

Living larvae were dechorionated, anaesthetized in 600 µM 3-aminobenzoic acid ethyl ester methanesulfonate in system-water with 1 µg/mL methylene blue, and mounted in 1 % low-melting-point agarose on a glass-bottom MetTek dish at specific stages. The larvae were maintained at 28 °C during imaging in a temperature-controlled stage top chamber (OKO Lab UNO-T). Images at successive focal depths were captured at 200 nm intervals and deconvolved with Microvolution software in ImageJ (NIH). The three-dimensional datasets were processed and volume-rendered with the surface evolver and filament-tracer tools in Imaris (Bitplane, Belfast, UK). The Imaris workstation was provided by the Rockefeller University Bio-imaging Resource Center.

Immunofluorescence microscopy

For the immunofluorescence labeling of wholemounted wild-type control and *sema7a$^{-/-}$* larvae, 1.5-4 dpf larvae were fixed overnight at 4 °C in 4 % formaldehyde in phosphate-buffered saline solution (PBS) with 1 % Tween-20 (1 % PBST). Larvae were washed four times with 1 % PBST for 15 min each, then placed for 2 hr in blocking solution containing PBS, 2 % normal donkey serum (NDS), 0.5 % Tween-20, and 1 % BSA. Primary antibodies were diluted in fresh blocking solution and incubated with the specimens overnight at 4 °C. The primary antibodies were goat anti-Sema7A (1:200; AF1835, R&D Systems) (14), rabbit anti-myosin VI (1:200; Proteus 25-6791), murine anti-GM130 (1:200; 610822, BD Transduction Laboratories), murine anti-CTBP (1:200; B-3, SC-55502, Santa Cruz Biotech), and rabbit anti-mCherry (1:200; GTX128508, GeneTex). Larvae were washed four times with 0.1% PBST for 15 min each. Alexa Fluor-conjugated secondary antibodies (Invitrogen, Molecular Probes) applied overnight at 1:200 dilutions in 0.2 % PBST included anti-rabbit (488 nm), anti-goat (555 nm), and anti-mouse (647 nm). Larvae were then washed four times in 0.2 % PBST for 15 min each and stored at 4 °C in VectaShield (Vector Laboratories). For the immunofluorescence labeling of postsynaptic density in wholemounted wild-type control and *sema7a$^{-/-}$* larvae, 2-4 dpf larvae were fixed with 4 % formaldehyde in PBS for 4.5-6 hr at 4 °C. Larvae were washed five times with 0.01 % PBST for 5 min each and then rinsed in distilled water for 5 min. The larvae were permeabilized with ice-cold acetone at -20 °C for 5 min. They were rinsed in distilled water for 5 min, washed five times with 0.01 % PBST for 5 min each, and blocked overnight with PBS buffer containing 2 % goat serum and 1 % BSA. Murine anti-pan-MAGUK

antibody (1:500; IgG1 NeuroMab, K28.86, 75-029) was diluted in PBS containing 1 % BSA, added to the larvae, and incubated for 3 hr at room temperature. Larvae were washed five times for 5 min each with 0.01 % PBST. Alexa Fluor 555-conjugated anti-mouse secondary antibody (1:1000) diluted in PBS containing 1 % BSA was added to the larvae and incubated for 2 hr at room temperature. Larvae were washed five times with 0.01 % PBST for 5 min each, rinsed in distilled water for 5 min, and stored at 4 °C in VectaShield (Vector Laboratories).

Posterior segments of fixed larvae were mounted on a glass slide and imaged with a microlens-based, super-resolution confocal microscope (VT-iSIM, VisiTech international) under 60X and 100X, silicone-oil objective lenses of numerical apertures 1.30 and 1.35, respectively. Images at successive focal depths were captured at 200 nm intervals and deconvolved with the Microvolution software in ImageJ.

Measurement of Sema7A intensity

The average Sema7A fluorescence intensities of the hair cells from 1.5 dpf, 2 dpf, 3 dpf, and 4 dpf neuromasts were measured by determining the mean gray level within each hair cell labeled by actin-GFP expression. The intensity distribution of Sema7A protein along the apicobasal axis of the hair cell was measured using the line profile tool in ImageJ (**Figure 1—figure supplement 1F**). Because hair cell lengths differed among samples, lines were drawn with 2 μm widths and varying lengths of 6-8 μm. For each hair cell, apicobasal length was scaled from 0 to 100 arbitrary units and the intensity values from 0 to 1 arbitrary units.

Generation of skeletonized networks

The labeled sensory axons were traced in three dimensions with ImageJ's semi-automated framework, SNT (48). Each trace depicts the skeletonized form of the posterior lateral-line nerve, the posterior lateral-line branch, and the point of arborization from which the sensory arbors radiate to contact the hair cells (**Fig. 2D,E**). The three-dimensional pixels or voxels obtained from the skeletonized sensory arbor traces were processed using custom code written in Python for visual representation and quantitative analysis.

Generation of combined hair cell clusters and the corresponding combined skeletonized networks

The hair cell clusters of neuromasts from each developmental stage were aligned by the centers of their apices, which were identified by the hair bundles, and overlayed to generate combined hair cell clusters using custom Python code. The associated skeletonized sensory-arbor traces at each developmental stage were aligned similarly using custom Python code. The details of the procedures are available upon request and the corresponding code is available on GitHub.

Quantification of sensory arbor distributions around hair cell clusters

The region from the center of the combined hair cell cluster to 60 μm in the post-cluster region was divided into 3600 concentric sections of equal area (**Figure 2—figure supplement 2A**). Each section, as depicted with a distinct color shade, had an area of π μm^2. Sensory arbor density was defined as Log_{10}[(Area occupied by the arbors in each section)/ (Area of each section)]. The arbor density was then plotted as a histogram against distance from the center of the combined hair cell cluster. Each bin of the histogram represents an area of π μm^2. The histograms were finally represented as density trace graphs with Kernel Density Estimation (KDE) in Python.

Quantification of contact between sensory arbors and hair cell clusters

For each hair cell cluster, the voxels of the sensory arbor traces that were inside or within 0.5 µm —the average neurite radius—of the cluster boundary were denoted as arbors in contact with their corresponding hair cell cluster (**Figure 2—figure supplement 2B**). The percentage of arbors in contact with each hair cell cluster was defined as: (Number of voxels that remained inside the cluster boundary/Total number of voxels in the arbor) X 100. The data were analyzed through an automated pipeline with custom code.

Quantification of the sensory arborization network topology

We developed a custom Python script (snt_topology.py; available on GitHub) to convert the skeletonized sensory arborization networks to network graphs (NetworkX, v3.1). We first used a custom ImageJ macro to convert SNT skeletons to csv files, then generated the network graph from the individual arbor paths. As noted previously, we defined five topological attributes: (1) nodes — junctions where arbors branch, converge, or cross; (2) loops—minimal arbor cycles forming topological holes; (3) bare terminals—arbors with free ends; (4) node degree—the number of first-neighbor nodes incident to a node; and (5) arbor curvature—the total curvature of a bare terminal (**Figure 3A**). To enumerate loops and quantify their lengths and node numbers, we computed the minimum cycle basis for each network graph. The relative organ height of each node in a graph was defined in 3D using **Equation (1)**:

$$(\vec{u} \cdot \vec{v}) \,/\, \|\vec{v}\|^2 , \qquad (1)$$

where u# is the vector from the arborization initiation point to a node and #v⃗ is the vector from the arborization initiation point to the hair cell cluster apex. The relative occurrence of nodes (**Figure 3—figure supplement 1A-C**) was normalized by both the number of hair cells per neuromast and the total number of neuromasts, for comparison across ages and genotypes. The relative number of bare terminals and loops (**Figure 3B**; **Figure 3—figure supplement 1D**, **E**) was normalized by the number of hair cells per neuromast and scaled between 0 and 1. The density was then normalized by the total number of neuromasts imaged for each developmental stage and genotype. For **Figure 3C** and **Figure 3—figure supplement 1F** and **G**, the normalized occurrence was computed as the number of arbors of a given length that formed either a bare terminal or a loop, divided by the total number of arbors of either feature of that length. Lastly, we defined bare terminals as having either high or low curvature (**Figure 3F**; **Figure 3—figure supplement 2C**, **D**) if their absolute total signed curvature [**Equation (2)**] in three dimensions was either higher or lower than $\pi/6$, respectively:

$$\left| \int \frac{dT}{ds} \cdot N(s)\, ds \right| , \qquad (2)$$

where s is the arc-length parameter of the bare terminal, $T(s)$ is the unit tangent vector at each point along the arbor, $N(s)$ is the unit normal vector at each point, and the integral is evaluated from the terminal's branching node to the arbor's tip. For a closed curve forming a full loop, this value will equal 2π . In practice, we first fit B-splines (scipy.interpolate.splprep; SciPy, v1.10.1) in 3D to the skeletons for each bare terminal before evaluating their derivatives (scipy.interpolate.splev) and integrating (scipy.integrate.simpson) over their lengths.

Quantification of aberrant sensory arborization in ectopic Sema7A^{sec} expression

The sensory arbor networks were traced in three dimensions with SNT. The surface of each of the ectopically expressing Sema7A^{sec}-mKate2 cells was represented by a single point that was closest to the terminal point of the guided neurite. Distances between two points were calculated using standard mathematical operations.

Statistical analysis

Data visualization and statistical analysis were conducted with GraphPad Prism (Version 9) and Python (v3.10). The Mann-Whitney test was used for hypothesis testing unless otherwise noted, and the statistical details are given in the respective figure legends.

Data and code availability

Owing to size restrictions, the experimental image data have not been uploaded to a repository but are available from the corresponding author on request. The code generated during this study is available on GitHub (*https://github.com/agnikdasgupta/Sema7A_regulates_neural_circuitry*).

Supporting information

Video 1

Video 2

Video 3

Video 4

Video 5

Video 6

Video 7

Video 8

Video 9

Video 10

Acknowledgements

The authors thank Nicolas Velez and Emily Atlas for valuable discussions. Samantha Campbell provided expert fish husbandry. Katie Kindt kindly provided various strains of zebrafish. Image processing benefitted from facilities at the Bio-Imaging Resource Center. A.D. was supported by a Kavli Neural Systems Institute Postdoctoral Fellowship from The Rockefeller University. C.C.R. is

supported by National Science Foundation Graduate Research Fellowship Grant No. 1946429. A.J., S.P.P., and L.M.S. were supported by Howard Hughes Medical Institute, of which A.J.H. is an Investigator.

Author Contributions

A.D. initiated the project, conducted experiments, analyzed data, and quantified results. C.C.R developed the Python codes for the network topology analysis and quantified those results, as well as analyzed published transcriptomics data. S.P.P. developed the Python codes for three-dimensional visual representation of sensory arbors and quantified arbor morphologies. L.M.S. conducted preliminary experiments. A.J. plotted Sema7A intensity measurements. A.D. wrote the paper with contributions from C.C.R and A.J.H.

Declaration of Interests

The authors declare no competing interests.

Figures and Figure Legends

Video 1. Sema7A is enriched at the hair cell base and sensory-axon interface. A through-focus scan of a 4 dpf control neuromast depicts the hair cells (green) that are innervated by the sensory axons (magenta) at their basolateral surfaces where the Sema7A protein (orange) is highly enriched. Scale bar, 5 μm.

Video 2. Three-dimensional arborization patterns in control and *sema7a*$^{-/-}$ neuromasts. Lateral views depict three-dimensionally rendered combined skeletonized network traces from 27 control and 27 *sema7a*$^{-/-}$ mutant neuromasts.

Video 3. Sensory axonal projections contact an embryonic muscle progenitor cell expressing Sema7A^{sec}. A through-focus scan of a 3 dpf larva depicts a muscle progenitor cell in the dermomyotome that expresses the ectopic Sema7A^{sec} (orange) and the sensory axonal projection (magenta) that makes intimate contact with it. Scale bar, 20 μm.

Video 4. Volumetric surface reconstruction of a sensory arbor and an embryonic muscle progenitor expressing Sema7A^{sec}. Reconstruction of the muscle progenitor cell (orange) at 3 dpf reveals its intimate association with an attracted sensory arbor (magenta).

Video 5. Sensory axonal projections remain in proximity to myofibers expressing Sema7A^{sec}. A through-focus scan of a 3 dpf larva depicts mature myofibers expressing exogenous Sema7A^{sec} deep in the myotome (orange) and the sensory axonal projection (magenta) that remains nearby.

Video 6. Volumetric surface reconstruction of a sensory arbor and the mature myofibers expressing Sema7A^{sec}. Reconstruction of mature myofibers expressing ectopic Sema7A^{sec} (orange) at 3 dpf shows their close association with the attracted sensory arbors (magenta).

Video 7. Aberrant axonal projections reenter the lateral-line nerve while following an ectopic Sema7A^{sec} source. A through-focus scan of a 3 dpf larva depicts cells expressing exogenous Sema7A^{sec} (orange) that guides the aberrant sensory axonal projection (magenta) back into the lateral-line nerve. Scale bar, 20 μm.

Video 8, 9, and 10. Ectopic Sema7A^{sec} expression induces aberrant neurite projections from the lateral-line nerve. Through-focus scans of 3 dpf larvae depict three individual incidents of ectopic *sema7a^{sec}* (orange) integrations that occurred distant from the neuromasts. In each case, myofibers express ectopic Sema7A^{sec} protein that attracts neurite extensions (arrowheads) from the lateral-line nerve (magenta). Scale bars, 20 μm.

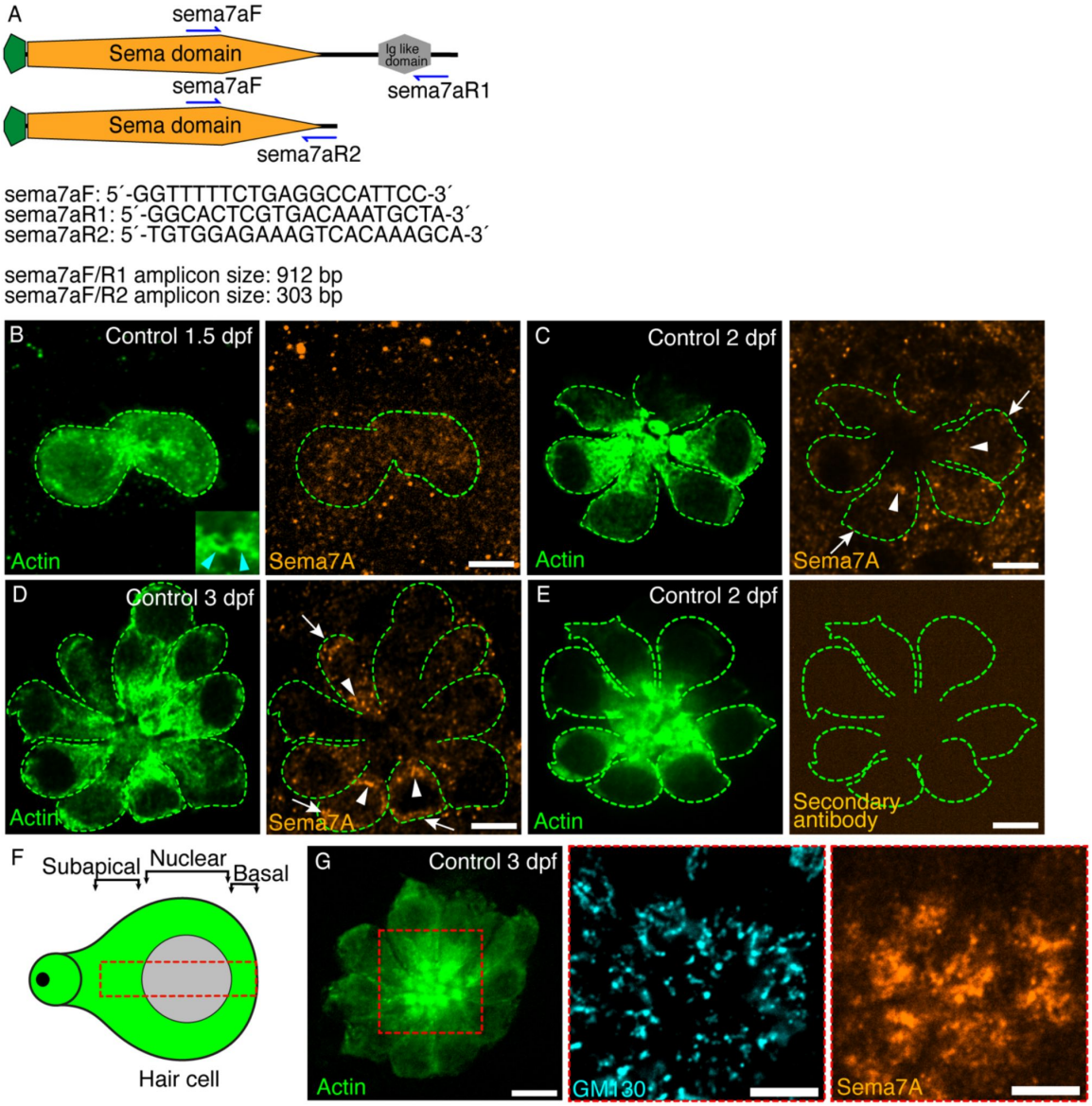

Figure 1—figure supplement 1.

Expression of Semaphorin7A in the lateral line neuromast.

(A) Distinct sets of primers (arrows) identify the two variants of the Sema7A protein molecule. (B-D) Surface micrographs show hair cells marked with actin-GFP (green dashed lines) and the localization of Sema7A protein (orange) in the subapical (arrowheads) and basal regions (arrows) of the corresponding hair cells from neuromasts of developing control larvae. The inset in panel B depicts the apices of the immature hair cell pair. (E) Immunolabeling with only the secondary antibody fails to detect any Sema7A signal. (F) A schematic diagram of a single hair cell depicts the three distinct regions along the apicobasal axis of the cell. Sema7A intensity was measured along this apicobasal axis (red dashed line). (G). A surface micrograph depicts hair cells (green, left) whose subapical region (red dashed line) harbors the Golgi network (cyan, middle) where the Sema7A protein is enriched (orange, right). Scale bars, 5 μm.

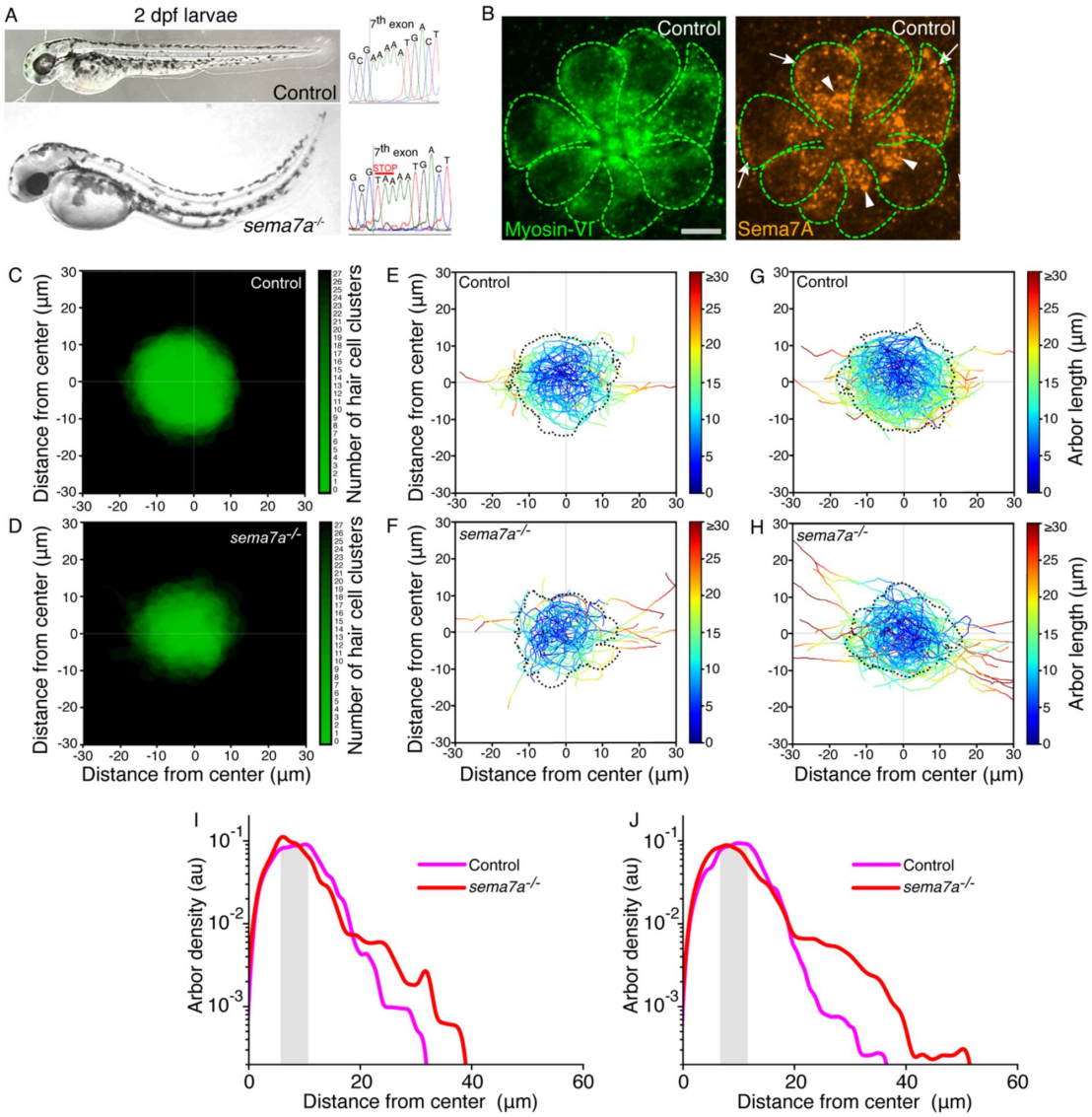

Figure 2—figure supplement 1.

sema7a$^{-/-}$ mutants exhibit aberrant sensory-axon arborization throughout development.

(A) Micrographs depict the overall morphologies and *sema7a* genomic profiles of 2 dpf control (top) and *sema7a*$^{-/-}$larvae (bottom). (B) In a surface micrograph of a 3 dpf control neuromast, myosin VI (green) marks hair cells (green dashed lines). Sema7A (orange) protein is highly enriched in the subapical region (arrowheads) and basolateral (arrow) region of the hair cells. (C,D) Micrographs depict combined 4 dpf hair cell clusters, each of whose centers arise located at (0,0). The X- and Y-coordinates represent the anteroposterior (AP) and dorsoventral (DV) axes of the larva, respectively. Positive values of the X- and Y-coordinates represent posterior and ventral directions, respectively. Combined hair cell clusters from 27 control and 27 *sema7a*$^{-/-}$ mutant neuromasts are represented. (E,F) Micrographs depict the skeletonized networks of the combined 2 dpf hair cell clusters from 17 control and 17 *sema7a*$^{-/-}$ mutant neuromasts. (G,H) Micrographs depict the skeletonized networks of the combined 3 dpf hair cell clusters from 29 control and 29 *sema7a*$^{-/-}$ mutant neuromasts. (I) A plot quantitates the densities of the sensory arbors around the center of the combined hair cell clusters for 33 control (magenta) and 17 *sema7a*$^{-/-}$(red) neuromasts at 2 dpf. The shaded area marks the region proximal to the boundary of the combined hair cell cluster. (J) A plot quantitates the densities of the sensory arbors around the center of the combined hair cell clusters for 29 control (magenta) and 53 *sema7a*$^{-/-}$ (red) neuromasts at 3 dpf. The shaded area marks the region proximal to the boundary of the combined hair cell cluster. Scale bar, 5 μm; au, arbitrary units.

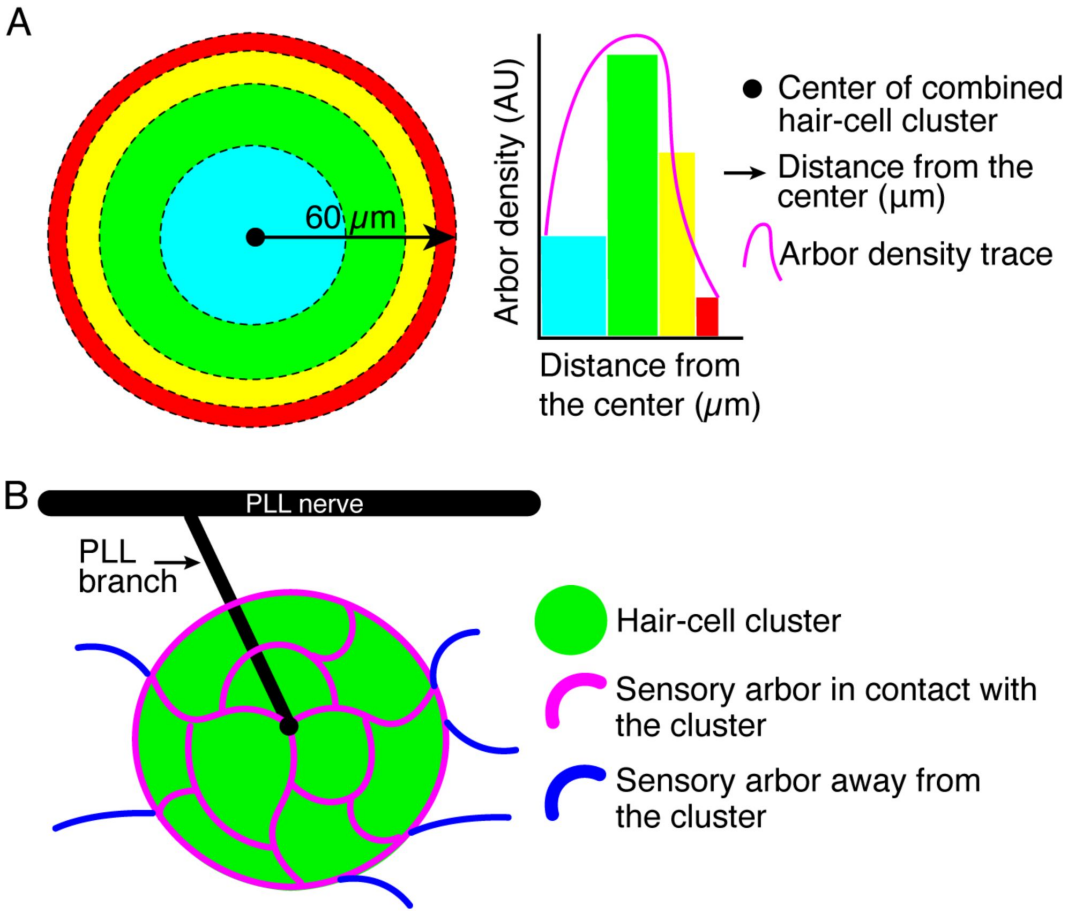

Figure 2—figure supplement 2.

Quantification of sensory arbor distributions and contacts with hair cell clusters.

(A) A schematic drawing of the combined hair cell cluster and surrounding region depicts concentric sections of equal area in distinct colors (cyan, green, yellow, and red). The arbor density is plotted as a histogram against the distance (black arrow) from the center (black circle) of the combined hair cell cluster. The histogram is represented as a density trace graph (magenta). (B) A schematic drawing of a posterior lateral-line neuromast depicts the posterior lateral-line (PLL) nerve (black), posterior lateral-line branch (black), the sensory arbors (magenta) that contact the hair cell cluster (green), and the sensory arbors that project away (blue) from the hair cell cluster.

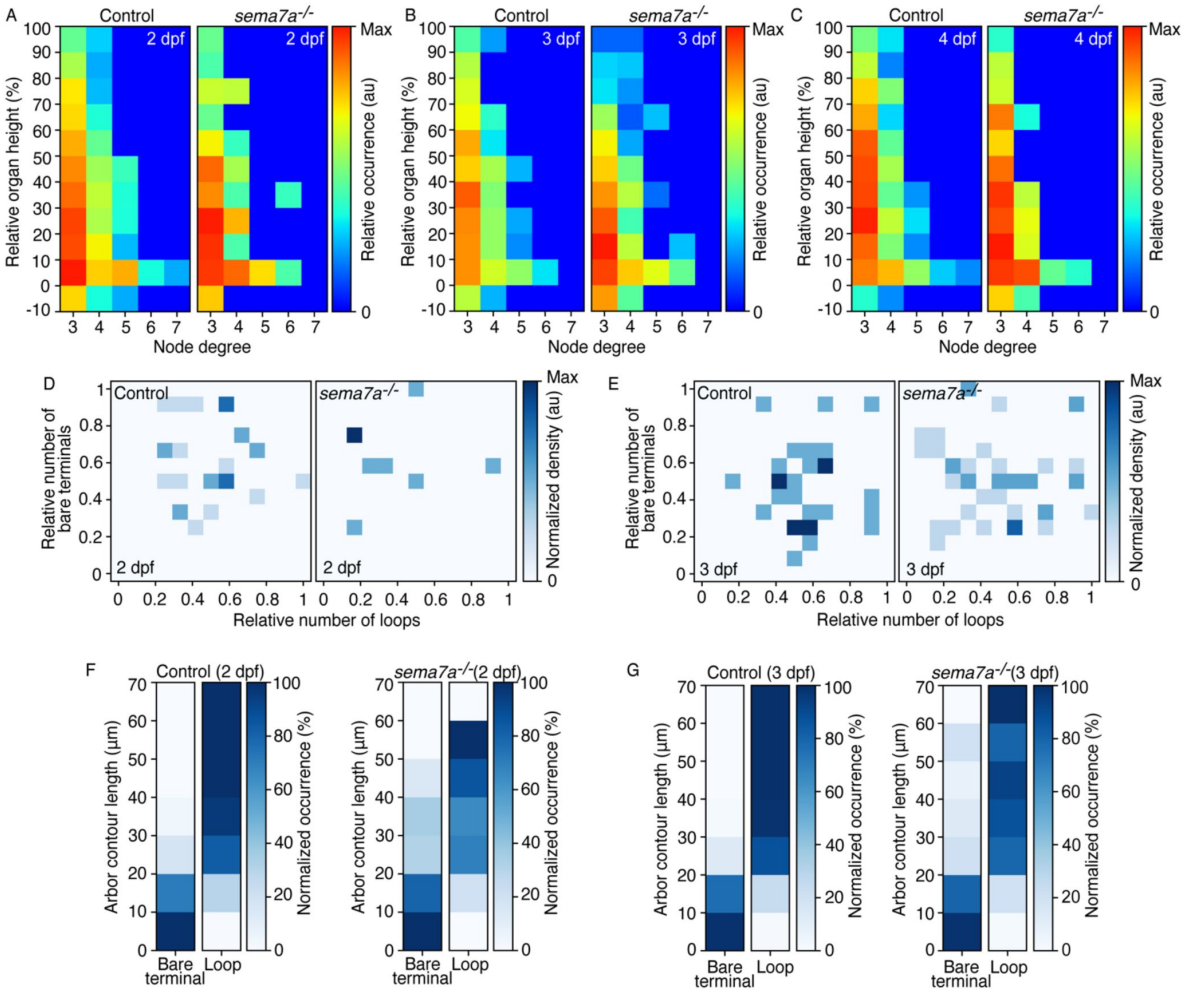

Figure 3—figure supplement 1.

Quantification of topological features across developmental stages and genotypes.

(A-C) The distribution of node degrees as a function of the height in hair cell clusters shows the difference in the network's hierarchical organization between control and *sema7a*$^{-/-}$ larvae. Nodes of low degree are commonly observed between genotypes across developmental stages (A, B), but their distribution along the cluster height became significantly different at 4 dpf (C), with nodes in control larvae localizing higher along the axis than in the mutants. In this and the following two panels, 33, 29, and 35 neuromasts were analyzed from 2 dpf, 3 dpf, and 4 dpf control larvae, respectively and 17, 53, and 27 neuromasts were analyzed from 2 dpf, 3 dpf, and 4 dpf *sema7a*$^{-/-}$ mutant larvae, respectively (D, E) The correlations between the relative number of bare terminals and loops from control and *sema7a*$^{-/-}$ neuromasts reveal dispersive distributions at both 2 dpf (D) and 3 dpf (E) stages, suggesting that the networks are undergoing reorganization and yet to adopt an ordered topology. (F, G) In the distribution of arbors between bare terminals and loops with respect to their contour lengths, mutants' arbors display significantly higher propensity to remain as bare terminals compared to the controls at both 2 dpf (F) and 3 dpf (G) stages. The samples were identical to those in the previous panel. Statistical analyses are displayed in **Table 1**.

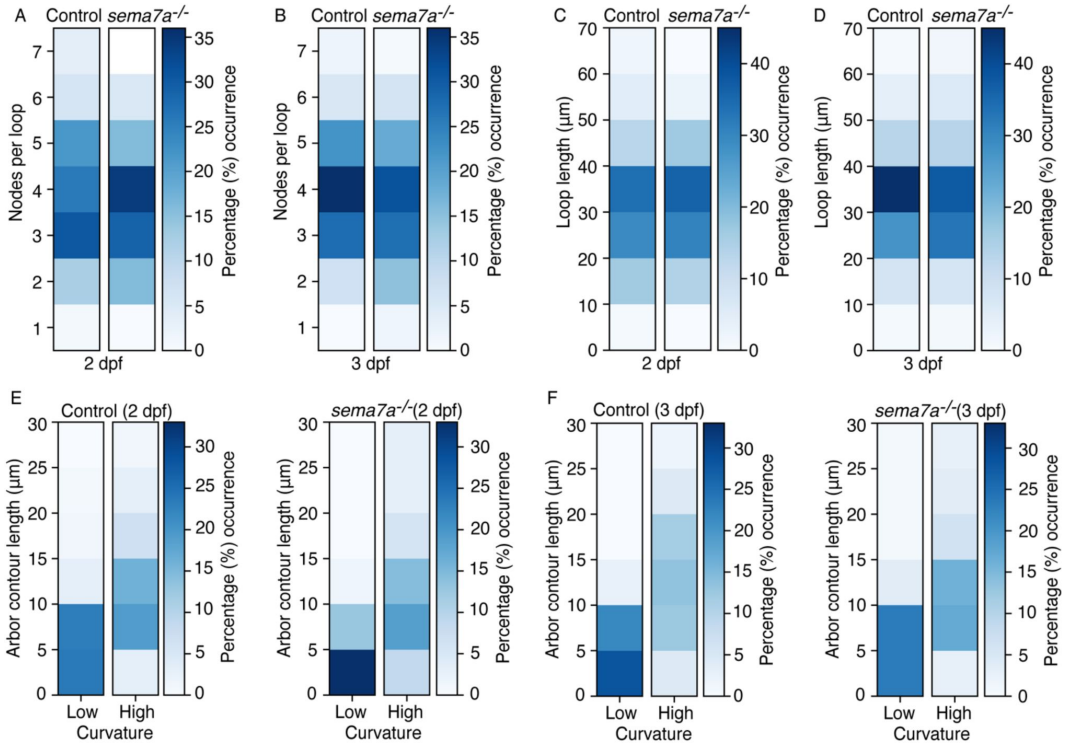

Figure 3—figure supplement 2.

Quantification of topological features between control and *sema7a*$^{-/-}$ larvae across developmental stages.

(A, B) Quantifications of the number of nodes per loop demonstrate a broader, but not significantly different, distribution in the mutants than the controls at both 2 dpf (A) and 3 dpf (B). In this and the following panels, 33 and 29 neuromasts were analyzed from 2 dpf and 3 dpf control larvae, respectively and 17 and 53 neuromasts were analyzed from 2 dpf and 3 dpf *sema7a*$^{-/-}$ mutant larvae, respectively. (C, D) Quantifications of loop lengths from the same larvae indicate a wider, but not significantly different, distribution in the mutants than the controls at both 2 dpf (C) and 3 dpf (D). (E, F) The distributions of bare terminals between low- and high-curvature groups from the same larvae show higher occurrences of long, curved arbors in the control and short, linear arbors in the mutants at both 2 dpf (E) and 3 dpf (F) stages. Statistical analyses are displayed in **Table 1**.

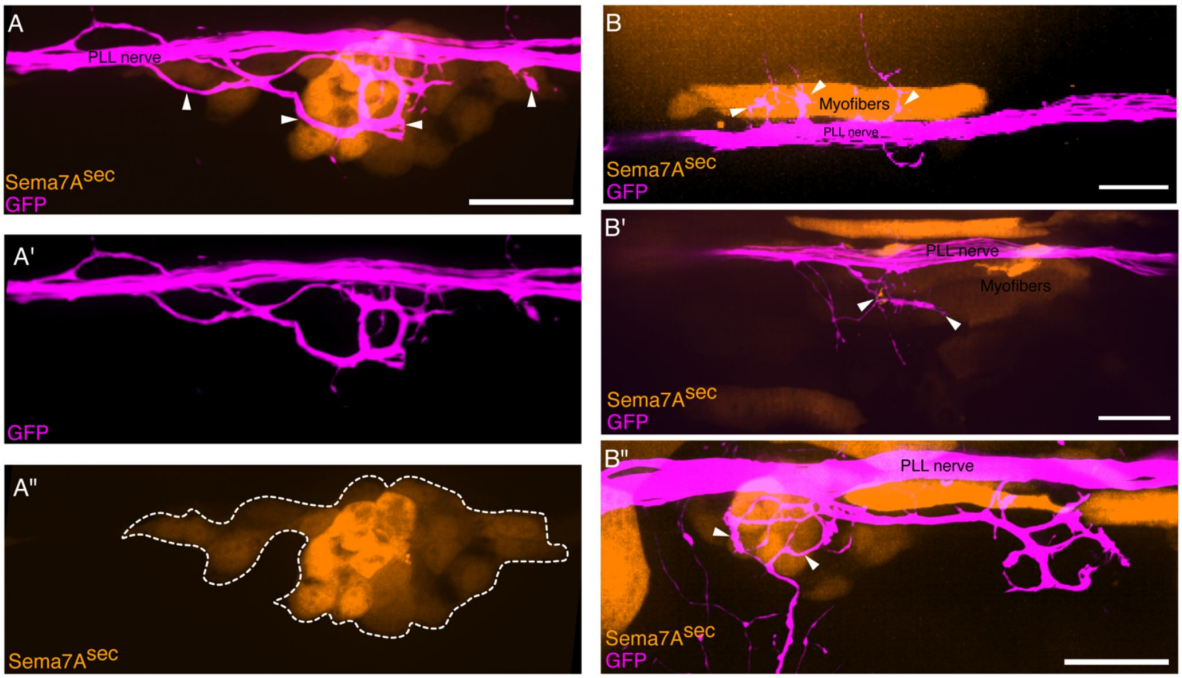

Figure 4—figure supplement 1.

Ectopic Sema7A^{sec} diffusive cues induce aberrant neural arborizations.

(A-A") In a micrograph of an ectopically expressing Sema7A^{sec} (orange) larva, the sensory arbors (magenta) extend multiple aberrant axonal projections (arrowheads) that reenter the lateral-line nerve while following an ectopic Sema7A source. Maximal-intensity projections of the sensory arbors and the ectopically expressing Sema7A cells (white dashed line) are shown in A' and A", respectively. (B-B") Micrographs depict three individual incidents of ectopic *sema7a^{sec}* (orange) integrations that occurred distant from neuromasts. In each case, a set of myofibers expresses the ectopic Sema7A^{sec} protein that induces neurite extensions (arrowheads) from the lateral-line nerve (magenta) toward itself. Scale bars, 20 µm.

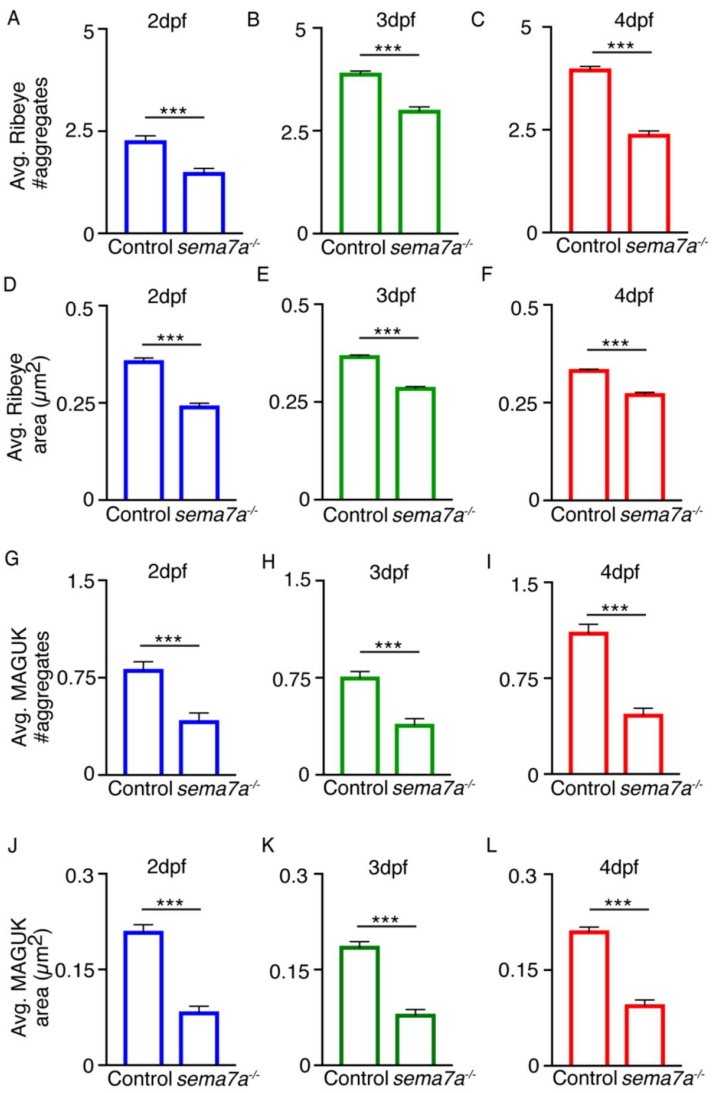

Figure 5—figure supplement 1.

sema7a$^{-/-}$ mutants display impaired synaptic assembly.

(A-F) The plots quantitate the average numbers and areas of presynaptic aggregates from control and *sema7a*$^{-/-}$ neuromasts. Significant decreases in the numbers and areas of presynaptic aggregates are observed across development. Three hundred and forty-one, 1229, and 1286 presynaptic aggregates were analyzed from 2 dpf, 3 dpf, and 4 dpf control larvae, respectively. Two hundred and thirty-five, 643, and 419 presynaptic aggregates were analyzed from 2 dpf, 3 dpf, and 4 dpf *sema7a*$^{-/-}$ mutant larvae, respectively. (G-L) The plots quantitate the average numbers and areas of postsynaptic aggregates from control and *sema7a*$^{-/-}$ neuromasts. Significant decreases in the numbers and areas of postsynaptic aggregates occurred during development. Three hundred and ninety-seven, 1243, and 1300 postsynaptic aggregates were analyzed from 2 dpf, 3 dpf, and 4 dpf control larvae, respectively. Three hundred and four, 651, and 451 postsynaptic aggregates were analyzed from 2 dpf, 3 dpf, and 4 dpf *sema7a*$^{-/-}$ mutant larvae, respectively. Means ± SEMs; *** implies $p < 0.001$.

References

1. Lykissas M, Batistatou A, Charalabopoulos K, Beris A (2007) **The Role of Neurotrophins in Axonal Growth, Guidance, and Regeneration** *Curr Neurovasc Res* **4**:143–51

2. Vaccaro G, Dumoulin A, Zuñiga NR, Bandtlow CE, Stoeckli ET (2022) **The Nogo-66 Receptors NgR1 and NgR3 Are Required for Commissural Axon Pathfinding** *J Neurosci* **42**:4087–100

3. Nguyen-Ba-Charvet KT, Di Meglio T, Fouquet C, Chedotal A (2008) **Robos and Slits Control the Pathfinding and Targeting of Mouse Olfactory Sensory Axons** *J Neurosci* **28**:4244–9

4. Pasterkamp R Jeroen, Peschon JJ, Spriggs MK, Kolodkin AL (2003) **Semaphorin 7A promotes axon outgrowth through integrins and MAPKs** *Nature* **424**:398–405

5. Nagiel A, Andor-Ardo D, Hudspeth AJ (2008) **Specificity of Afferent Synapses onto Plane-Polarized Hair Cells in the Posterior Lateral Line of the Zebrafish** *J Neurosci* **28**:8442–53

6. Jacobo A, Dasgupta A, Erzberger A, Siletti K, Hudspeth AJ (2019) **Notch-Mediated Determination of Hair-Bundle Polarity in Mechanosensory Hair Cells of the Zebrafish Lateral Line** *Curr Biol* **29**:3579–3587

7. Valera G, Markov DA, Bijari K, Randlett O, Asgharsharghi A, Baudoin JP, et al. (2021) **A neuronal blueprint for directional mechanosensation in larval zebrafish** *Curr Biol* **31**:1463–1475

8. Dow E, Jacobo A, Hossain S, Siletti K, Hudspeth AJ (2018) **Connectomics of the zebrafish's lateral-line neuromast reveals wiring and miswiring in a simple microcircuit** *eLife* **7**

9. Lush ME, Diaz DC, Koenecke N, Baek S, Boldt H, St Peter MK, et al. (2019) **scRNA-Seq reveals distinct stem cell populations that drive hair cell regeneration after loss of Fgf and Notch signaling** *eLife* **8**

10. Carulli D, de Winter F, Verhaagen J (2021) **Semaphorins in Adult Nervous System Plasticity and Disease** *Front Synaptic Neurosci* **13**

11. Yazdani U, Terman JR (2006) **The semaphorins** *Genome Biol* **7**:211

12. de Winter F, Kwok JCF, Fawcett JW, Vo TT, Carulli D, Verhaagen J (2016) **The Chemorepulsive Protein Semaphorin 3A and Perineuronal Net-Mediated Plasticity** *Neural Plast* **2016**:1–14

13. Coate TM, Spita NA, Zhang KD, Isgrig KT, Kelley MW (2015) **Neuropilin-2/Semaphorin-3F-mediated repulsion promotes inner hair cell innervation by spiral ganglion neurons** *eLife* **4**

14. Carcea I, Patil SB, Robison AJ, Mesias R, Huntsman MM, Froemke RC, et al. (2014) **Maturation of cortical circuits requires Semaphorin 7A** *Proc Natl Acad Sci* **111**:13978–83

15. Inoue N, Nishizumi H, Naritsuka H, Kiyonari H, Sakano H (2018) **Sema7A/PlxnCl signaling triggers activity-dependent olfactory synapse formation** *Nat Commun* **9**:1842

16. Inoue N, Nishizumi H, Ooyama R, Mogi K, Nishimori K, Kikusui T, et al. (2021) **The olfactory critical period is determined by activity-dependent Sema7A/PlxnC1 signaling within glomeruli** *eLife* **10**

17. Morote-Garcia JC, Napiwotzky D, Köhler D, Rosenberger P (2012) **Endothelial Semaphorin 7A promotes neutrophil migration during hypoxia** *Proc Natl Acad Sci* **109**:14146–51

18. Nishide M, Kumanogoh A (2018) **The role of semaphorins in immune responses and autoimmune rheumatic diseases** *Nat Rev Rheumatol* **14**:19–31

19. Köhler D, Granja T, Volz J, Koeppen M, Langer HF, Hansmann G, et al. (2020) **Red blood cell-derived semaphorin 7A promotes thrombo-inflammation in myocardial ischemia-reperfusion injury through platelet GPIb** *Nat Commun* **11**:1315

20. Pham TL, He J, Kakazu AH, Jun B, Bazan NG, Bazan HEP (2017) **Defining a mechanistic link between pigment epithelium–derived factor, docosahexaenoic acid, and corneal nerve regeneration** *J Biol Chem* **292**:18486–99

21. Xie J, Wang H (2017) **Semaphorin 7A as a potential immune regulator and promising therapeutic target in rheumatoid arthritis** *Arthritis Res Ther* **19**:10

22. Dow E, Siletti K, Hudspeth AJ (2015) **Cellular projections from sensory hair cells form polarity-specific scaffolds during synaptogenesis** *Genes Dev* **29**:1087–94

23. Pujol-Martí J, Faucherre A, Aziz-Bose R, Asgharsharghi A, Colombelli J, Trapani JG, et al. (2014) **Converging Axons Collectively Initiate and Maintain Synaptic Selectivity in a Constantly Remodeling Sensory Organ** *Curr Biol* **24**:2968–74

24. De Wit J, De Winter F, Klooster J, Verhaagen J (2005) **Semaphorin 3A displays a punctate distribution on the surface of neuronal cells and interacts with proteoglycans in the extracellular matrix** *Mol Cell Neurosci* **29**:40–55

25. Ji YR, Warrier S, Jiang T, Wu DK, Kindt KS (2018) **Directional selectivity of afferent neurons in zebrafish neuromasts is regulated by Emx2 in presynaptic hair cells** *eLife* **7**

26. Diaz-Horta O, Abad C, Sennaroglu L, Foster J, DeSmidt A, Bademci G, et al. (2016) **ROR1 is essential for proper innervation of auditory hair cells and hearing in humans and mice** *Proc Natl Acad Sci U S A* **113**:5993–8

27. Newman M (2018) **The structure of real-world networks [Internet]** *[cited 2023 May 2]. Available from* https://academic.oup.com/book/27884/chapter/203817512

28. Sharma P, Ruel TD, Kocha KM, Liao S, Huang P (2019) **Single cell dynamics of embryonic muscle progenitor cells in zebrafish** *Development*

29. Keenan SR, Currie PD (2019) **The Developmental Phases of Zebrafish Myogenesis** *J Dev Biol* **7**:12

30. Sato A, Koshida S, Takeda H (2010) **Single-cell analysis of somatotopic map formation in the zebrafish lateral line system** *Dev Dyn* **239**:2058–65

31. Shen K, Cowan CW (2010) **Guidance Molecules in Synapse Formation and Plasticity** *Cold Spring Harb Perspect Biol* **2**:a001842–a001842

32. Um JW, Ko J (2017) **Neural Glycosylphosphatidylinositol-Anchored Proteins in Synaptic Specification** *Trends Cell Biol* **27**:931–45

33. Uesaka N, Uchigashima M, Mikuni T, Nakazawa T, Nakao H, Hirai H, et al. (2014) **Retrograde semaphorin signaling regulates synapse elimination in the developing mouse brain** *Science* **344**:1020–3

34. Sheets L, Hagen MW, Nicolson T, Riley B (2014) **Characterization of Ribeye Subunits in Zebrafish Hair Cells Reveals That Exogenous Ribeye B-Domain and CtBP1 Localize to the Basal Ends of Synaptic Ribbons** *PLoS ONE* **9**:e107256

35. Oliva C, Escobedo P, Astorga C, Molina C, Sierralta J (2012) **Role of the maguk protein family in synapse formation and function** *Dev Neurobiol* **72**:57–72

36. Suli A, Pujol R, Cunningham DE, Hailey DW, Prendergast A, Rubel EW, et al. (2016) **Innervation regulates synaptic ribbons in lateral line mechanosensory hair cells** *J Cell Sci* :182592

37. Taschenberger H, Leão RM, Rowland KC, Spirou GA, von Gersdorff H (2002) **Optimizing Synaptic Architecture and Efficiency for High-Frequency Transmission** *Neuron* **36**:1127–43

38. Myers JP, Gomez TM (2011) **Focal Adhesion Kinase Promotes Integrin Adhesion Dynamics Necessary for Chemotropic Turning of Nerve Growth Cones** *J Neurosci* **31**:13585–95

39. O'Donnell M, Chance RK, Bashaw GJ (2009) **Axon Growth and Guidance: Receptor Regulation and Signal Transduction** *Annu Rev Neurosci* **32**:383–412

40. Gilmour D, Knaut H, Maischein HM, Nüsslein-Volhard C (2004) **Towing of sensory axons by their migrating target cells in vivo** *Nat Neurosci* **7**:491–2

41. Metcalfe WK (1985) **Sensory neuron growth cones comigrate with posterior lateral line primordial cells in zebrafish** *J Comp Neurol* **238**:218–24

42. Gasanov EV, Rafieva LM, Korzh VP, Proost P (2015) **BDNF-TrkB Axis Regulates Migration of the Lateral Line Primordium and Modulates the Maintenance of Mechanoreceptor Progenitors** *PLOS ONE* **10**:e0119711

43. Schuster K, Dambly-Chaudière C, Ghysen A (2010) **Glial cell line-derived neurotrophic factor defines the path of developing and regenerating axons in the lateral line system of zebrafish** *Proc Natl Acad Sci* **107**:19531–6

44. Germanà A, Laurà R, Montalbano G, Guerrera MC, Amato V, Zichichi R, et al. (2010) **Expression of Brain-Derived Neurotrophic Factor and TrkB in the Lateral Line System of Zebrafish During Development** *Cell Mol Neurobiol* **30**:787–93

45. Kindt KS, Finch G, Nicolson T (2012) **Kinocilia Mediate Mechanosensitivity in Developing Zebrafish Hair Cells** *Dev Cell* **23**:329–41

46. Obholzer N, Wolfson S, Trapani JG, Mo W, Nechiporuk A, Busch-Nentwich E, et al. (2008) **Vesicular Glutamate Transporter 3 Is Required for Synaptic Transmission in Zebrafish Hair Cells** *J Neurosci* **28**:2110–8

47. Kwan KM, Fujimoto E, Grabher C, Mangum BD, Hardy ME, Campbell DS, et al. (2007) **The Tol2kit: A multisite gateway-based construction kit forTol2 transposon transgenesis constructs** *Dev Dyn* **236**:3088–99

48. Arshadi C, Günther U, Eddison M, Harrington KIS, Ferreira TA (2021) **SNT: a unifying toolbox for quantification of neuronal anatomy** *Nat Methods* **18**:374–7

Author information

Agnik Dasgupta
Howard Hughes Medical Institute and Laboratory of Sensory Neuroscience, The Rockefeller University, New York, NY, USA
ORCID iD: 0000-0003-0860-1006

Corresponding author: Dr. Agnik Dasgupta Laboratory of Sensory Neuroscience The Rockefeller University New York, NY 10065 Telephone: 212-327-7353 E-mail: adasgupta@rockefeller.edu

Caleb C. Reagor
Howard Hughes Medical Institute and Laboratory of Sensory Neuroscience, The Rockefeller University, New York, NY, USA, Tri-Institutional PhD Program in Computational Biology and Medicine, New York, NY, USA
ORCID iD: 0000-0002-8304-1267

Sang P. Paik[3]
Howard Hughes Medical Institute and Laboratory of Sensory Neuroscience, The Rockefeller University, New York, NY, USA

[3]Department of Functional Neuroanatomy, Institute for Anatomy and Cell Biology, Heidelberg University, Heidelberg, Germany

Lauren M. Snow[4]
Howard Hughes Medical Institute and Laboratory of Sensory Neuroscience, The Rockefeller University, New York, NY, USA

[4]Brigham and Women's Hospital, Boston, MA, USA

Adrian Jacobo
Howard Hughes Medical Institute and Laboratory of Sensory Neuroscience, The Rockefeller University, New York, NY, USA, Chan Zuckerberg Biohub San Francisco, San Francisco, CA, USA
ORCID iD: 0000-0001-9381-6292

A. J. Hudspeth
Howard Hughes Medical Institute and Laboratory of Sensory Neuroscience, The Rockefeller University, New York, NY, USA
ORCID iD: 0000-0002-0295-1323

Editors

Reviewing Editor
David Raible
University of Washington, Seattle, United States of America

Senior Editor
Didier Stainier
Max Planck Institute for Heart and Lung Research, Bad Nauheim, Germany

Reviewer #1 (Public Review):

In this work, Dasguta et al. have dissected the role of Sema7a in fine tuning of a sensory microcircuit in the posterior lateral line organ of zebrafish. They attempt to also outline the different roles of a secreted verses membrane-bound form of Sema7a in this process. Using genetic perturbations and axonal network analysis, the authors show that loss of both Sema7a isoforms causes abnormal axon terminal structure with more bare terminals and fewer loops in contact with presynaptic sensory hair cells. Further, they show that loss of Sema7a causes decreased number and size of both the pre- and post-synapse. Finally, they show that overexpression of the secreted form of Sema7a specifically can elicit axon terminal outgrowth to an ectopic Sema7a expressing cell. Together, the analysis of Sema7a loss of function and overexpression on axon arbor structure is fairly thorough and revealed a novel role for Sema7a in axon terminal structure. However, the connection between different isoforms of Sema7a and the axon arborization needs to be substantiated. Furthermore, an autocrine role for Sema7a on the presynaptic cell is not ruled out as a contributing factor to the synaptic and axon structure phenotypes. Finally, critical controls are absent from the overexpression paradigm. These issues weaken the claims made by the authors including the statement that they have identified differential roles for the GPI-anchored verses secreted forms of Sema7a on synapse formation and as a chemoattractant for axon arborization respectively. The manuscript itself would benefit from the inclusion of details in the text to help the reader interpret the figures, tools, data, and analysis.

https://doi.org/10.7554/eLife.89926.1.sa3

Reviewer #2 (Public Review):

In this work, Dasgupta et al. investigates the role of Sema7a in the formation of peripheral sensory circuit in the lateral line system of zebrafish. They show that Sema7a protein is present during neuromast maturation and localized, in part, to the base of hair cells (HCs). This would be consistent with pre-synaptic Sema7a mediating formation and/or stabilization of the synapse. They use sema7a loss-of-function strain to show that lateral line sensory terminals display abnormal arborization. They provide highly quantitative analysis of the lateral line terminal arborization to show that a number of specific topological parameters are affected in mutants. Next, they ectopically express a secreted form of Sema7a to show that lateral line terminals can be ectopically attracted to the source. Finally, they also demonstrate that the synaptic assembly is impaired in the sema7a mutant. Overall, the data are of high quality and properly controlled. The availability of Sema7a antibody is a big plus, as it allows to address the endogenous protein localization as well to show the signal absence in the sema7a mutant. The quantification of the arbor topology should be useful to people in the field who are looking at the lateral line as well as other axonal terminals. I think some results are overinterpreted though. The authors state: "Our findings demonstrate that Sema7A functions both as a juxtracrine and as a secreted cue to pattern neural circuitry during sensory organ development." However, they have not actually demonstrated which

isoform functions in HCs (also see comments below). In addition, they have to be careful in interpreting their topology analysis, as they cannot separate individual axons. Thus, such analysis can generate artifacts. They can perform additional experiments to address these issues or adjust their interpretations.

https://doi.org/10.7554/eLife.89926.1.sa2

Reviewer #3 (Public Review):

Summary:

This study demonstrates that the axon guidance molecule Sema7a patterns the innervation of hair cells in the neuromasts of the zebrafish lateral line, as revealed by quantifying gain- and loss-of function effects on the three-dimensional topology of sensory axon arbors over developmental time. Alternative splicing can produce either a diffusible or membrane-bound form of Sema7a, which is increasingly localized to the basolateral pole of hair cells as they develop (Figure 1). In sema7a mutant zebrafish, sensory axon arbors still grow to the neuromast, but they do not form the same arborization patterns as in controls, with many arbors overextending, curving less, and forming fewer loops even as they lengthen (Figure 2,3). These phenotypes only become significant later in development, indicating that Sema7a functions to pattern local microcircuitry, not the gross wiring pattern. Further, upon ectopic expression of the diffusible form of Sema7a, sensory axons grow towards the Sema7a source (Figure 4). The data also show changes in the synapses that form when mutant terminals contact hair cells, evidenced by significantly smaller pre- and post-synaptic punctae (Figure 5). Finally, by replotting single cell RNA-sequencing data (Figure 6), the authors show that several other potential cues are also produced by hair cells and might explain why the sema7a phenotype does not reflect a change in growth towards the neuromast. In summary, the data strongly indicate that Sema7a plays a role in shaping connectivity within the neuromast.

Strengths:

The main strength of this study is the sophisticated analysis that was used to demonstrate fine-level effects on connectivity. Rather than asking "did the axon reach its target?", the authors asked "how does the axon behave within the target?". This type of deep analysis is much more powerful than what is typical for the field and should be done more often. The breadth of analysis is also impressive, in that axon arborization patterns and synaptic connectivity were examined at 3 stages of development and in three-dimensions.

Weaknesses:

The main weakness is that the data do not cleanly distinguish between activities for the secreted and membrane-bound forms of Sema7a, which the authors speculate may influence axon growth and synapse formation respectively. The authors do not overstate the claims, but it would have been nice to see some additional experimentation along these lines, such as the effects of overexpressing the membrane-bound form, some analysis of the distance over which the "diffusible" form of Sema7a might act (many secreted ligands are not in fact all that diffusible), or some live-imaging of axons before they reach the target (predicted to be the same in control and mutants) and then within the target (predicted to be different). Clearly, although the gain-of-function studies show that Sema7a can act at a distance, other cues are sufficient. Although the lack of a phenotype could be due to compensation, it is also possible that Sema7a does not actually act in a diffusible manner within its natural context.

Overall, the data support the authors' carefully worded conclusions. While certain ideas are put forward as possibilities, the authors recognize that more work is needed. The main

shortcoming is that the study does not actually distinguish between the effects of the two forms of Sema7a, which are predicted but not actually shown to be either diffusible or membrane linked (the membrane linkage can be cleaved). Although the study starts by presenting the splice forms, there is no description of when and where each splice form is transcribed. Additionally, since the mutants are predicted to disrupt both forms, it is a bit difficult to disentangle the synaptic phenotype from the earlier changes in circuit topology - perhaps the change at the level of the synapse is secondary to the change in topology. Further, the authors do not provide any data supporting the idea that the membrane bound form of Sema7a acts only locally. Without these kinds of data, the authors are unable to attribute activities to either form.

The main impact on the field will be the nature of the analysis. The field of axon guidance benefits from this kind of robust quantification of growing axon trajectories, versus their ability to actually reach a target. This study highlights the value of more careful analysis and as a result, makes the point that circuit assembly is not just a matter of painting out paths using chemoattractants and repellants, but is also about how axons respond to local cues. The study also points to the likely importance of alternative splice forms and to the complex functions that can be achieved using different forms of the same ligand.

https://doi.org/10.7554/eLife.89926.1.sa1

Reviewer #4 (Public Review):

Summary:
The work by Dasgupta et al identifies Sema7a as a novel guidance molecule in hair cell sensory systems. The authors use the both genetic and imaging power of the zebrafish lateral-line system for their research. Based on expression data and immunohistochemistry experiments, the authors demonstrate that Sema7a is present in lateral line hair cells. The authors then examine a sema7a mutant. In this mutant, Sema7a proteins levels are nearly eliminated. Importantly, the authors show that when Sema7a is absent, afferent terminals show aberrant projections and fewer contacts with hair cells. Lastly the authors show that ectopic expression of the secreted form of Sema7a is sufficient to recruit aberrant terminals to non-hair cell targets. The sema7a innervation defects are well quantified. Overall, the paper is extremely well written and easy to follow.

Strengths:
1. The axon guidance phenotypes in sema7a mutants are novel, striking and thoroughly quantified.
2. By combining both loss of function sema7a mutants and ectopic expression of the secreted form of Sema7a the authors demonstrate the Sema7a is both necessary and sufficient to guide sensory axons

Weaknesses:
1. Control. There should be an uninjected heatshock control to ensure that heatshock itself does not cause sensory afferents to form aberrant arbors. This control would help support the hypothesis that exogenously expressed Sema7a (via a heatshock driven promoter) is sufficient to attract afferent arbors.
2. Synapse labeling. The numbers obtained for postsynaptic labeling in controls do not match up with the published literature - they are quite low. Although there are clear differences in postsynaptic counts between sema7a mutants and controls, it is worrying that the numbers are so low in controls. In addition, the authors do not stain for complete synapses (pre- and post-synapses together). This staining is critical to understand how Sema7a impacts synapse formation.
3. Hair cell counts. The authors need to provide quantification of hair cell counts per neuromast in mutant and control animals. If the counts are different, certain quantification

may need to be normalized.
4. Developmental delay. It is possible that loss of Sema7a simply delays development. The latest stage examined was 4 dpf, an age that is not quite mature in control animals. The authors could look at a later age, such as 6 dpf to see if the phenotypes persist or recover.

https://doi.org/10.7554/eLife.89926.1.sa0